AN ASSESSMENT OF MAGNETIZATION EFFECTS ON HYDROGEN CRACKING FOR THICK WALLED PIPELINES

ANNUAL PROGRESS REPORT

1. INTRODUCTION

The pipeline network in the Beaufort Sea of Alaska is conservatively designed to protect against thermal effects, ice mechanics, and environmental concerns. To satisfy these conditions, pipeline is constructed from thick wall pipes and high strength steels generally covered by the American Petroleum Institute Specification 5L. Since the integrity of the pipelines is nowadays monitored using inspection tools called pigging tools, Beaufort Sea's pipeline system requires a high level of confidence and reliance on inspection techniques. The updated high technology In-Line Inspection tools are called intelligent pigging tools, and the Magnetic Flux Leakage (MFL) tool is the most valuable to assess metal loss and currently useful to detect mechanical damages. This technique is performed by magnetizing the pipe wall and then detecting a local flux leakage caused by anomalies relative to change in pipe wall thickness.

As theoretically demonstrated in the Project Progress Report (March 31, 2004), the diffusible hydrogen content in steels will be affected by a magnetic field. It brings to light the fact that the hydrogen concentration in pipeline steels would be significantly affected by the magnetization produced during pigging operations. If the diffusible hydrogen concentration increases under magnetization conditions, the potential of enhanced hydrogen cracking could be observed. Indeed, hydrogen induced cracking susceptibility in pipeline steels increases as the material strength increases.

The MFL tools use strong permanent magnets to create a uniform, consistent magnetic flux density in the pipeline steel up to the magnetic saturation. At localized anomalies such as metal loss and mechanical damage, the magnetic flux leaks out from the pipe, which is immediately detected by an electronic sensor. The magnetic saturation of pipeline steels depends upon the material strength and the wall thickness of the pipe. The number and power of the permanent magnets positioned in the MFL tool define the applied magnetic flux density.

Four fundamental variables have been defined to evaluate how a strong magnetic flux density produced throughout recurrent pigging routines affect the hydrogen-induced cracking susceptibility of thick walled and high-strength pipeline steels. These variables are pipeline steel grade, wall thickness, residual stress effect, and magnetic flux density. Because pipelines in the Beaufort Sea (Alaska) utilize high strength steel grades up to API Spec. 5L Grade X80, the experimental approach

plans to use three steel grades: X52, X70, and X80. The wall thickness range of the selected pipeline samples is from $^5/_{16}$ to ¾ inches (7.94 to 19.0 mm).

This annual research report presented to the Department of the Interior (D.O.I.) and the Department of Transportation (D.O.T.) of the United States of America contains a description of the experimental approach, progress report, and the future plan. The experimental approach section presents an enlightenment of the steel characterization technique, the hydrogen charging and magnetic flux density application methods, as well as the electrochemical techniques primarily used to achieve the main focus of this project. The progress results show evidence of the effect of strong magnetic flux density on the diffusible hydrogen absorption rate in pipeline steels. Finally, the future work section essentially describes the methodology to accomplish the hydrogen-induced cracking susceptibility in pipeline steels, the measurement of hydrogen permeability and diffusivity using electrochemical techniques, and the steel surface change due to hydrogen content.

2. OBJECTIVES

The main objective of this annual research report is to present the progress results and the field testing plans designed to evaluate the effect of the magnetic flux density generated by MFL inspection tools on the diffusible hydrogen activity in thick walled, high strength pipeline steels. To achieve this assessment, electrochemical cathodic charging and permeability cells, magnet-setup tools, and residual stress methods have already been designed and employed. Although the progress results point to the fact that the total hydrogen absorption rate in high-strength pipeline steels increases under high magnetic flux density, the magnetization effect either on hydrogen permeability or on the hydrogen-induced cracking susceptibility has been planned for future work. If the augmented level of total hydrogen is determined to be deleterious, possible corrective actions will be assessed, such as modified cathodic protection system and/or use of demagnetization tools following pigging.

3. MILESTONE CHART

Since the project start date, August 1st - 2003, nine of fifteen defined research tasks have been completed to date. The total hydrogen absorption rate using an electrochemical cathodic charging cell without magnetic field and under high magnetic flux density has been measured. These steel samples were obtained from all API Grades unloaded and loaded to various levels of stress using tensile test specimens. The electrochemical cell to measure hydrogen permeability and diffusivity was designed and employed with preliminary steel samples. The milestone description and completion date information is presented in the following chart.

No.	TASK	Completion Date
1.	**Literature review** of pigging operation and data, field data analysis and visit of field pigging operation; understand the salient differences of Beaufort Sea offshore application.	Aug 31, 2003
2.	Selection and procurement of pipeline steel grades X-42 and X-52 in 3/8" thick wall sections, heat treatment, analysis and microstructural investigation and hydrogen charging equipment set-up: Electrochemical cathodic charging	Nov 30, 2003
3.	Hydrogen charging and measurement of the amount of hydrogen absorbed (without magnetic field).	Dec 31, 2003
4.	Design and fabrication of (a) Devanathan and (b) Barnacle Hydrogen Permeability measurement equipment	Feb 29, 2004
5.	Measurement of hydrogen by Seebeck Method and the Vibrating Magnetometer.	Mar 31, 2004
6.	Submission of Progress Report	Mar 31, 2004
7.	Design and fabrication of high strength magnetic field setup for hydrogen charging, charging and measurement of the amount of hydrogen absorbed.	July 30, 2004
8.	Procurement of high strength line pipe steels; X-70 and X-80 in ¾" wall thickness	Aug 31, 2004
9.	Measurement of residual stress effect on hydrogen absorption. Steel samples will be loaded to various levels of stress.	Oct 31, 2004
10.	Report: Year 1 and submission of field testing plans	Nov. 30, 2004

11.	Determination of hydrogen induced cracking in all samples:
	    (a) Steel grade (strength)
	    (b) Residual stress (simulated by external loading: Task 9)
	Correlate hydrogen content, magnetic field and hydrogen cracking susceptibility.
	Measurement of hydrogen permeability and diffusivity by Devanathan and Barnacle Electrode Cells.
		May 31, 2005

12	**MMS-DOT-CSM Meeting for status update and Mod-II project discussions.**	Jun 30, 2005
13.	Potentiodynamic polarization measurements to investigate steel surface change due to hydrogen content on the cathodic absorption of hydrogen during pigging.	Aug 31, 2005
14.	Simulation of field conditions and determination of cracking in steels.	Oct 31, 2005
15.	Preparation of draft report	Nov30, 2005
16.	Submission of final report	**Dec 31, 2005**

4. THEORETICAL BASICS

Although the progress report submitted in March 2004 suggests the relationship between hydrogen concentration and magnetization in a similar manner, the next expression details the basics. This description leads to a graphical technique of the relationship.

A thermodynamic expression of equilibrium is utilized to derive the relationship between the thermoelectric power coefficient and the activity of hydrogen. Beginning with the first law of thermodynamics and assuming a reversible process:

$$dE = TdS - PdV - \delta w_{ext}$$

[1]

where S is the entropy, T is the temperature, P is the pressure, V is the volume, and w_{ext} is the external work done by the system.

At constant pressure (dP=0), enthalpy is introduced as the sum of the internal energy and the product of pressure and volume (H=E+PV). Differentiating enthalpy and incorporating into Equation 1 gives:

$$dH = TdS - \delta w_{ext}$$

[2]

Equation 2 is inserted into the differential Gibb's free energy (dG=dH-SdT-TdS) given as:

$$dG = -\delta w_{ext} - SdT + \sum \mu_i n_i$$

[3]

where the $\sum \mu_i n_i$ is additional free energy accounting for the addition of alloying elements to the solution (in this case, hydrogen).

Because the hydrogen concentration in pipeline steel is measured after an electrochemical reaction (cathodic charging), an electrochemical component must be included. Therefore, in a reversible process, the external work term is given as:

$$\delta w_{ext} = -\Delta M \, B - n_e FE \tag{4}$$

where ΔM is the change in magnetization and B is the magnetic field strength or magnetic flux density.

Now assume that the external work is magnetic work and is performed isothermally and by analogy to the thermodynamics of a reversible cell Equation 3 then becomes:

$$dG = -\Delta M \, B - n_e FE + \sum \mu_i n_i \tag{5}$$

where the $\sum \mu_i n_i$ is additional free energy accounting for the addition of alloying elements to the solution (in this case, hydrogen) and where the chemical potential of species i is given by $\mu_i = \mu_i^o + RT \ln a$. That is;

$$dG = -\Delta M \, B - n_e FE + \sum \mu_i^o n_i + \sum RTLna \tag{6}$$

Consider the region of hydrogen solubility where the appropriate reaction, in terms of electrochemistry, is given as:

$$2H^+ + 2e^- \rightarrow 2H(s) \tag{7}$$

Where H(s) is a hydrogen atom in solid solution in the solid metal matrix. Therefore, Equation 6 becomes:

$$dG = -\Delta M \, B - n_e FE + \sum \mu_i^o n_i + RTLn\left(\frac{[H]^2}{[H^+]^2} \right) \tag{8}$$

Rearranging:

$$dG = -\Delta M \, B - n_e FE + \sum \mu_i n_i + 2RTLn[H] + 2RT(pH) \tag{9}$$

Assuming equilibrium conditions, dG=0 and solving Equation 9 for the change in magnetization as a function of hydrogen content gives:

$$\Delta M = -\frac{n_e FE}{B} + \frac{\sum \mu_i n_i}{B} + \left(\frac{2RT}{B}\right) Ln[H] + \left(\frac{2RT}{B}\right) 2.3 pH \tag{10}$$

In contrast, solving Equation 9 for the hydrogen concentration as a function of magnetization gives:

$$Ln[H] = \left(\frac{\Delta M}{2RT}\right) B + \left(\frac{n_e FE}{2RT}\right) - \left(\frac{1}{2RT}\right) \sum \mu^o{}_i n_i - 2.3 pH \tag{11}$$

Standard state for hydrogen dissociation reaction is:

$$\varepsilon^o = \frac{\sum \mu^o{}_i n_i}{RT} \tag{12}$$

Consequently, Equation 11 becomes:

$$Ln[H] = \left(\frac{\Delta M}{2RT}\right) B + \left(\frac{FE}{RT}\right) - \frac{\varepsilon^o}{2} - 2.3 pH \tag{13}$$

When B=0, then [H] is the equilibrium hydrogen content without a magnetic field called $[H]_{B=0}$. Putting Equation 13 into exponential form:

$$[H]_{B=0} = \exp\left(\frac{FE}{RT} - \frac{\varepsilon^o}{2} - 2.3 pH\right) \tag{14}$$

Under a magnetic flux density, the hydrogen content is determined by:

$$[H]_{B=B} = [H]_{B=0} * \exp\left(\frac{\Delta M}{2RT}\right)B$$

[15]

Equation 15 shows how the absorbed hydrogen concentration increases with magnetic flux experience. This expression says that the hydrogen solubility will increase exponentially with increasing magnetic flux.

Rearranging Equation 15, the graphical expression is founded on Equation 16 where the slope of the straight line is a material property under experimental conditions, as following:

$$Ln[H]_{B=B} = Ln[H]_{B=0} + \left(\frac{\Delta M}{2RT}\right)B$$

[16]

Figure 1 shows the relationship of the hydrogen concentration as a function of the magnetic field.
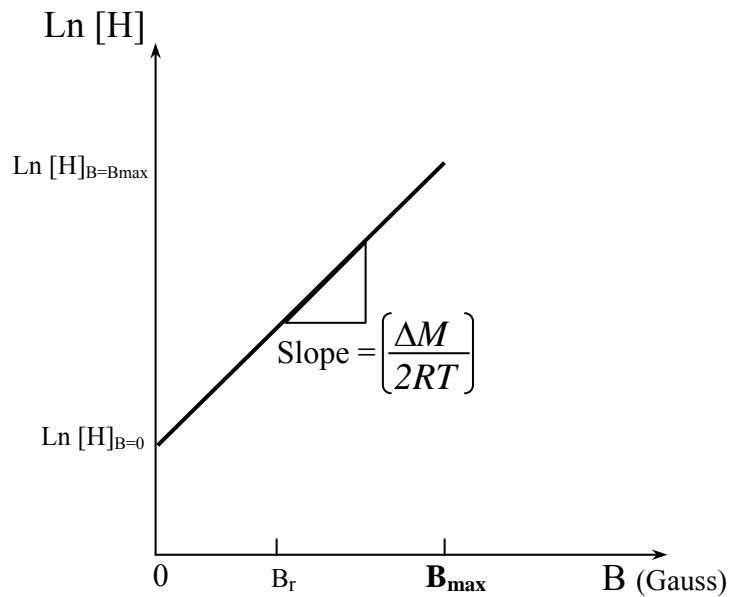
Figure 1. Schematic representation of Equation 16.

5.   EXPERIMENTAL APPROACH

a.   Characterization of Pipeline Steel Samples

Because the steel pipe samples (API Grade X52 and X70), obtained from a local energy company were unidentified, a set of standardized tests was run to verify their mechanical properties and chemical compositions. The tests are performed according to API Spec 5L testing procedure, which refers to the requirements of ASTM A370. Microstructural analysis was required to complete the characterization of the as-received material.

i. <u>Tensile test</u>

Four standard size tensile test specimens from large-diameter tubular products are cut from both steel pipes; two specimens from each steel grade, X52 and X70. The tensile tests were run according to the API Spec 5L requirements using the material test system MTS Alliance RT/100 (Fig. 2). The nominal load capacity of the system is 100 kN (22,500 lbs). Table 1 shows the mechanical properties of the steel tested (Fig. 3) in this study, and the properties of the specified steel as per API Spec. 5L requirements.

Figure 2. Load Measurement System - Tensile Test Machine

Table 1. Mechanical properties of tested steel X52 and X70.

Sample	API Spec. 5L Requirements		Tensile Test	
	Yield Strength Minimum psi (MPa)	UTS Minimum psi (MPa)	Yield Strength psi (MPa)	UTS psi (MPa)
X52 – a	52,000 (358.5)	66,000 (455.0)	78,998 (544.7)	80,523 (555.2)
X52 – b			72,227	83,020

			(498.0)	(572.4)
X70 – a	70,000 (482.6)	82,000 (565.4)	81,892 (564.6)	94,893 (654.3)
X70 – b			83,346	93,429
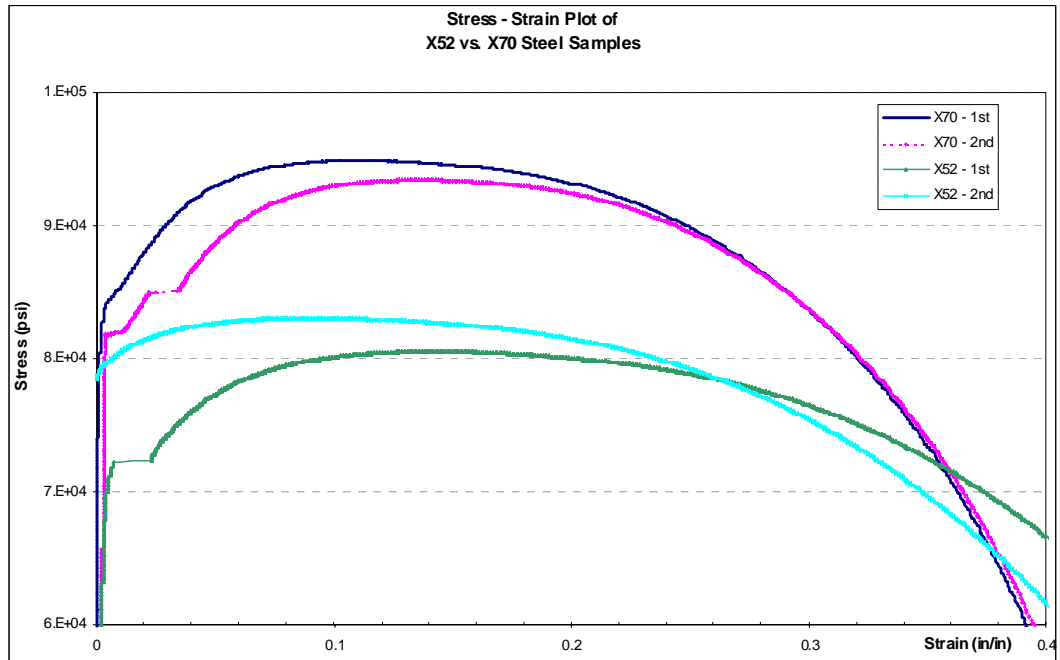
Figure 3. Tensile test diagram of tested steel, X52 and X70.

ii. Microstructure and Chemical Composition

The microstructures of all the samples were examined using standard optical microscopy, where typical photomicrographs are shown in Figure 4. The X52 pipeline steel sample exhibited equiaxed ferrite/low-pearlite microstructure typical of heat-treated, micro-alloyed steels with grain sizes ranging from 4 to 20 μm (Fig. 4 a-b). The X70 pipeline steel sample also displayed a ferrite/low-pearlite microstructure but with slightly more refined grain sizes ranging from 3 to 12 μm (Fig. 4 c-d). The elongated nature of the grains reflecting the rolling direction and texturing are evident in these micrographs.

The steel samples used for the laboratory tests were low carbon steel, produced according to API 5L Grade X52 and X70 specifications. Table 2 shows the chemical composition of the steel tested in this study, and for the steel matching the API Spec. 5L requirements.
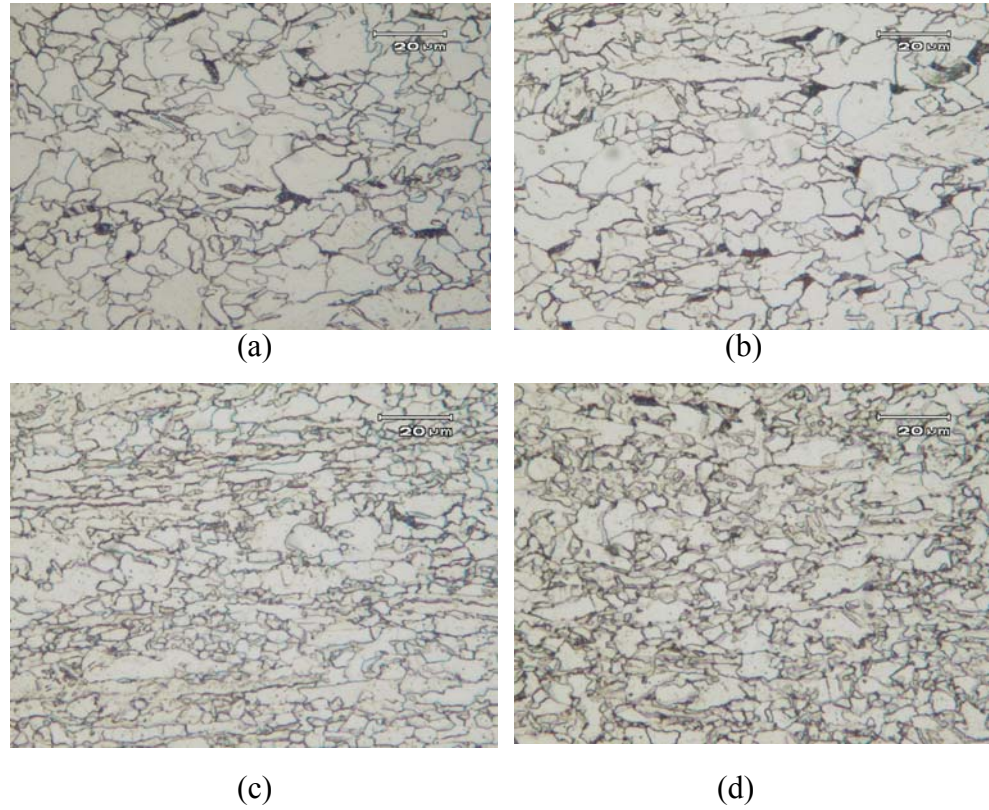
(a)

(b)

(c)

(d)

Figure 4. Microphotography of both X52 (a-b) and X70 (c-d) steel samples showing a ferrite/pearlite microstructure. Longitudinal sections, (a) and (c). Transversal sections, (b) and (d).

Table 2. Chemical composition of tested steel, X52 and X70.

Material	Carbon (%)	Manganese (%)	Phosphorus (%)	Sulfur (%)
X52 Tested Steel	0.0610	1.31	0.005	0.0069
	0.0609	1.30	0.004	0.0069
	0.0606	1.31	0.005	0.0073
X70 Tested Steel	0.0740	1.41	0.012	0.0029
	0.0655	1.41	0.005	0.0033
	0.0718	1.42	0.012	0.0031
API X52	0.30 max.	1.35 max.	0.04 max.	0.05 max.
API X70	0.23 max.	1.60 max.	0.04 max.	0.05 max.

b.   Magnetic Flux Density

The magnetizing system of the Magnetic Flux Leakage (MFL) tool creates a magnetic field in the pipeline steel near the saturation flux density that interacts with anomalies to produce local changes (leakage) in this applied field close to the pipe's surface. Commonly, the pipeline materials (low-carbon steels) are soft-ferromagnetic alloys. The parameters of saturation (B_s or M_s), remanent magnetization (B_r or M_r) and coercivity (H_c) of these steels depend, primarily, of the particular chemical composition, heat and rolling treatment, residual stresses, and density of inclusions. On the other hand, the induced magnetic field intensity is affected by other parameters such as variation of characteristics of magnet-pipe wall contact, MFL tool velocity, and remnant flux density (Fig. 5). Remanence, which is a measure of the remaining magnetization when the driving field is dropped to zero (0 kOe), is the most influential factor proposed in this work.

A rule of thumb estimates that approximately three times the value of the steel coercivity (H_c) is needed to magnetize common low carbon steels for the purpose of magnetic testing. However, detailed research has found values for the magnetization that are outside of the typical value ranges. These typical values for industrial steels are: B_s = 1.4-1.8 Tesla, H_c = 3.5 – 20 Oe, and B_r = 0.3-1.5 Tesla.

To establish the magnetic flux density required to saturate the X52 and X70 steel samples, a magnetic properties test was run in the Electronics and Electrical Engineering Laboratory – Electromagnetic Division of the National Institute of Standards and Technology (NIST) in Boulder, CO. Magnetization hysteresis loops were measured with a transverse-field vibrating-sample magnetometer at room temperature in maximum applied fields of 0.6 T (600 Gauss). Magnetization was computed as magnetic moment per unit mass of metal and expressed in units of Kilogauss.
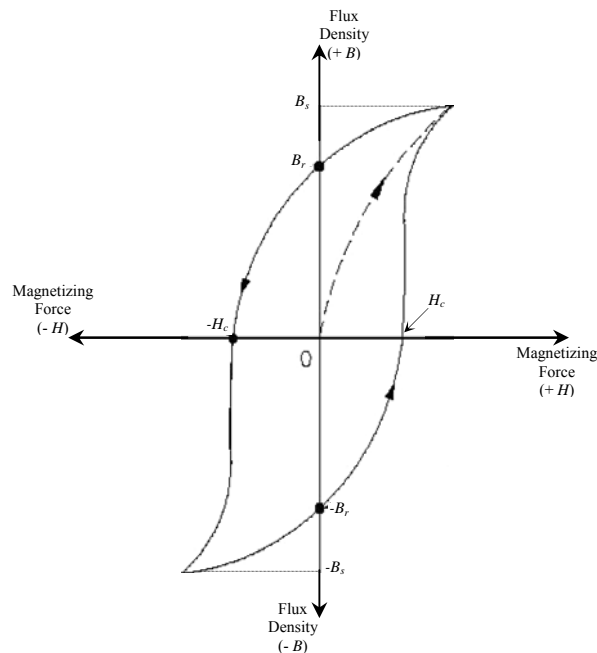
Figure 5. Hysteresis loop where the degree of retained magnetization (B_r) in ferromagnetic materials (pipeline steel) is illustrated.

Figure 6a shows the magnetization curves obtained from the test. The saturation magnetic flux density (B_s) for the longitudinal samples is approximately 1.8 Tesla (18,000 Gauss) and for the radial or transverse samples is 1.6 Tesla (16,000 Gauss). Notice that in the radial direction of the pipe the maximum saturation magnetic field density (B_{sR}) of both steels, X52 and X70, is slightly greater than in the longitudinal direction (B_{sL}), due to the rolling texturing obtained in the tested specimens. Moreover, the magnetic field required to saturate the steel in the radial direction (H_{sR}) is significantly lower than the field needed in the longitudinal direction (H_{sL}) of the pipe. The radial-direction B_{sR} is slightly larger than the longitudinal-direction B_{sL}, most likely because of the test specimen shape; while H_{sR} is considerably lower then H_{sL} because of the orientation of grains after hot rolling.

On the other hand, the remanence points of pipeline steel grade X52 is showed in Figure 6b. Remaining magnetic flux density in both lateral and radial directions is approximately 1 Tesla (10,000 Gauss). This parameter clearly shows a strong influence when experimental results are analyzed.
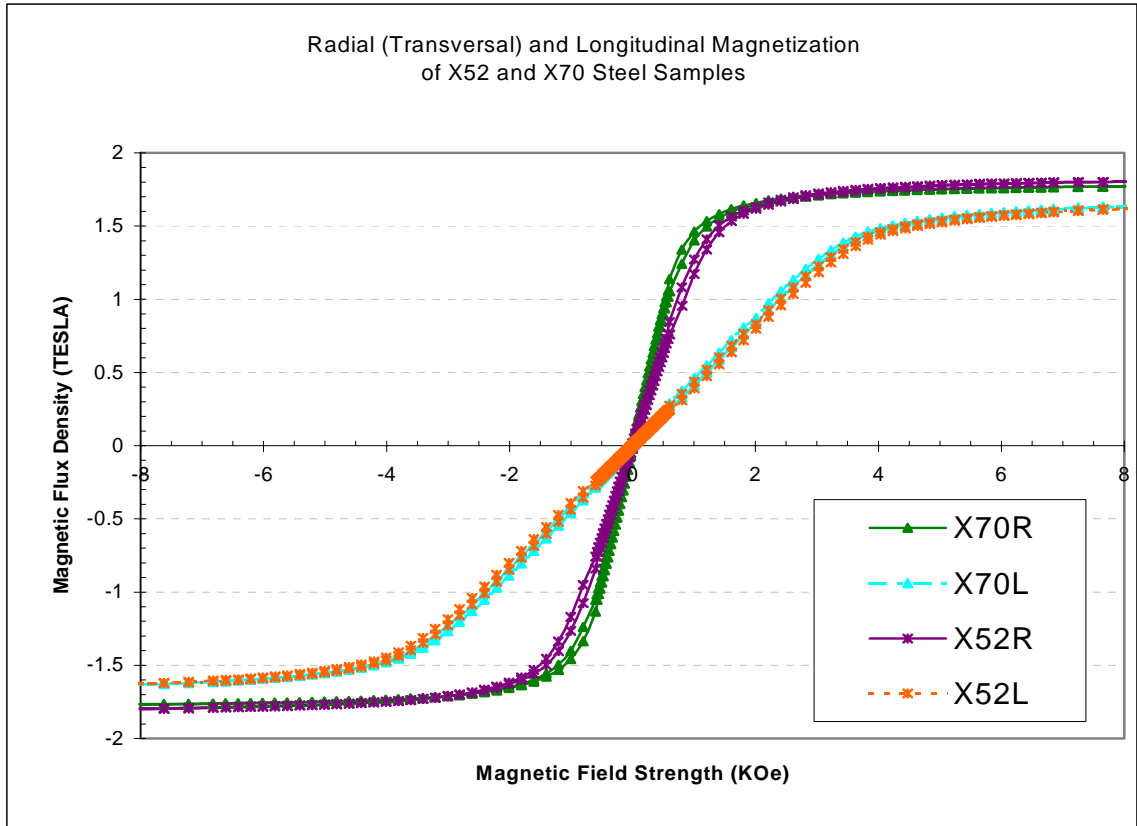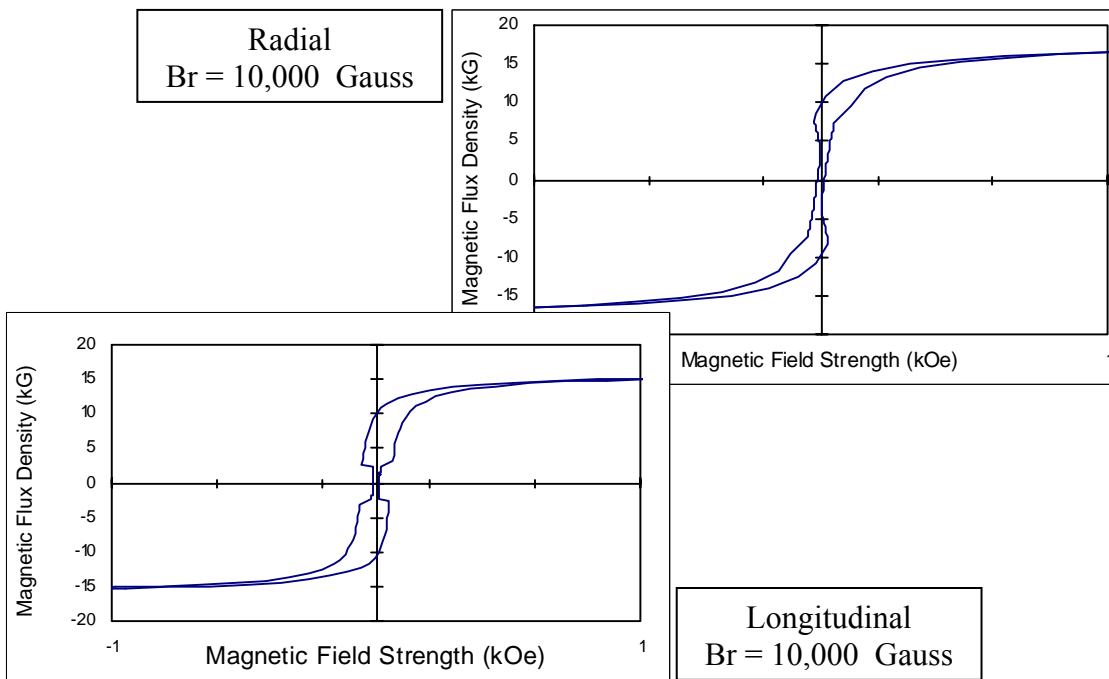
Figure 6a. Magnetization test results

Figure 6b. Remaining Magnetic Flux Density (Br) – Steel Grade X52

To reach the saturation flux density on the steel samples, an electromagnet based upon Biot-Savart law was initially constructed as a magnetic induction source. The electromagnet was made using a pure iron rod and a wrapped, high electric conductivity-isolated wire, which an electrical current passes through. However, the maximum magnetic flux density measured from this straight electromagnet was inadequate, lower than 500 Gauss. Because of the dimensional limitations of the electrochemical cathodic charging cell, a C-shape electromagnet is inappropriate. A high-resolution 0-2 Tesla Gauss meter records the measurements.

Therefore strong permanent magnets, like those used in Magnetic Flux Leakage In-Line Inspection tools, were chosen as the magnetic induction source of the magnetic drive system. Unique configuration of larger pyramid-shape and smaller square-shape and circular-shape magnets constitute the magnet setup (Fig. 7). This individual configuration generates a magnetic induction greater than 0.97 Tesla (9,700 Gauss) (Fig.8).

With the purpose of increasing the magnetic flux density of the system, two similar configurations are bonded as north-south pole. The assembly of these permanent magnets produces a magnetic induction greater than 1.9 Tesla (19,000 Gauss). This value is large enough to saturate the high strength pipeline steel samples.
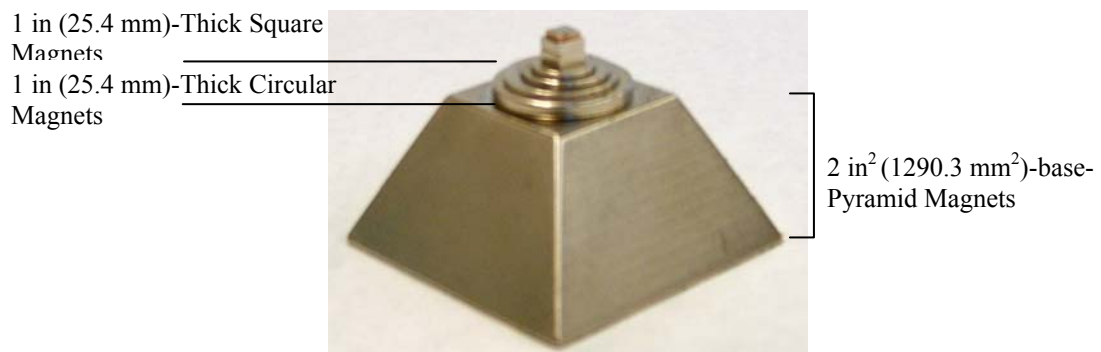

1 in (25.4 mm)-Thick Square Magnets

1 in (25.4 mm)-Thick Circular Magnets

$2 \ in^2 (1290.3 \ mm^2)$-base-Pyramid Magnets

Figure 7. Magnet configuration. Larger $2 \ in^2$ (1290.3 mm^2)-pyramid-shape magnet and smaller circular-shape and square -shape magnets.
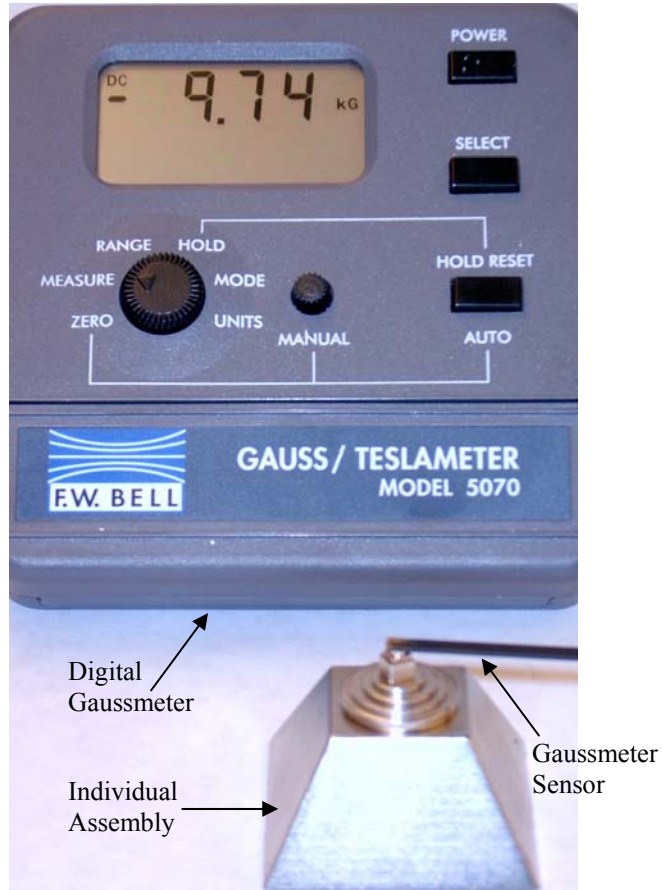
Figure 8. The individual assembly of pyramid and small permanent magnets generates a strong magnetic flux density: 0.96 Tesla (9,600 Gauss).

It is well understood that the magnetic field must be strong enough to produce the saturation magnetic flux density commonly used in Magnetic Flux Leakage In-Line Inspection tools. These inspection tools use a series of permanent magnets located near the internal surface of the pipe to magnetically saturate the steel and detect anomalies.

c. Magnet Set-up Frame

Because the individual set of permanent magnets generates a strong magnetic flux density at the top of the assembly, the force due to the north-south pole attraction is extremely high. This attraction force between the two sets of permanent magnets is not possible to be handled manually. As an unexpected experimental approach, initial setting-up methods cause the damage of some small magnets. This unpredicted collision between the permanent magnets destroys some of the small 1 mm (0.039 in)-thick square-shaped and circular-shaped magnets. With the intention of preventing more destruction of small magnets and uncontrolled setting-up methods, an engineering design concept is employed. An aluminum base magnet-setup frame achieves the safe and controllable sample-magnet assemblage.

Principles of mechanical engineering and screw-powered systems are considered for designing the frame. Figures 9 through 12 illustrate the engineering drawings to be used for constructing the assembly tool. Two principal notched, guided 1 in (25.4 mm)-thick aluminum sheets hold the two sets of permanent magnets that are both bonded and separated by action of a power screw. The selected material for the power screw and bearing box, based upon availability and cost, is low carbon steel. This inflexible selection creates another engineering problem: the magnetic attraction of them to the magnets. The magnetic attraction between the magnets and the powered system is reduced only by distance. A 1 in (25.4 mm)-thick and a ½ in (12.7 mm)-thick aluminum sheets separate them sufficiently to manually control the magnet setting.

This magnet-setup frame (Fig. 13) designed on campus and constructed by an experienced machine shop, reduced considerably the sample-magnet set-up time. This particular method reduces up to ten (10) times the setup timing required manually. Moreover, no more magnets will be destroyed during their collision as a result of the strong magnetic attraction forces.

With the purpose of determining the magnetic flux density saturating the pipeline steel samples, the Gauss meter sensor is placed between it and the permanent magnets. The recorded magnetic induction value exceeds the digital Gauss meter range: 2 Tesla – 20,000 gauss (Fig. 14). The achieved magnetic flux density value is greater than the saturation (B_s) value obtained from the magnetization tests (Fig. 6a).
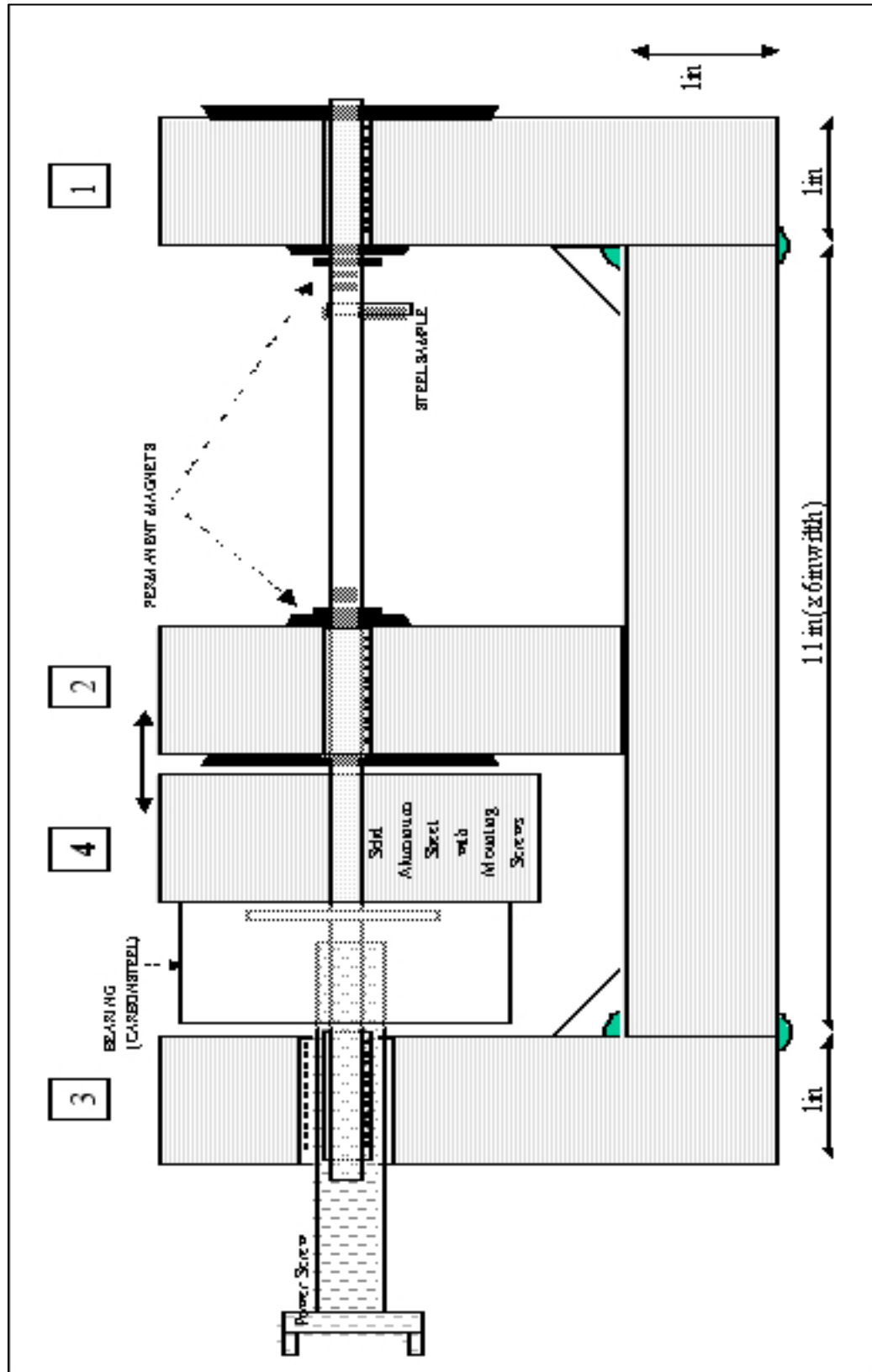
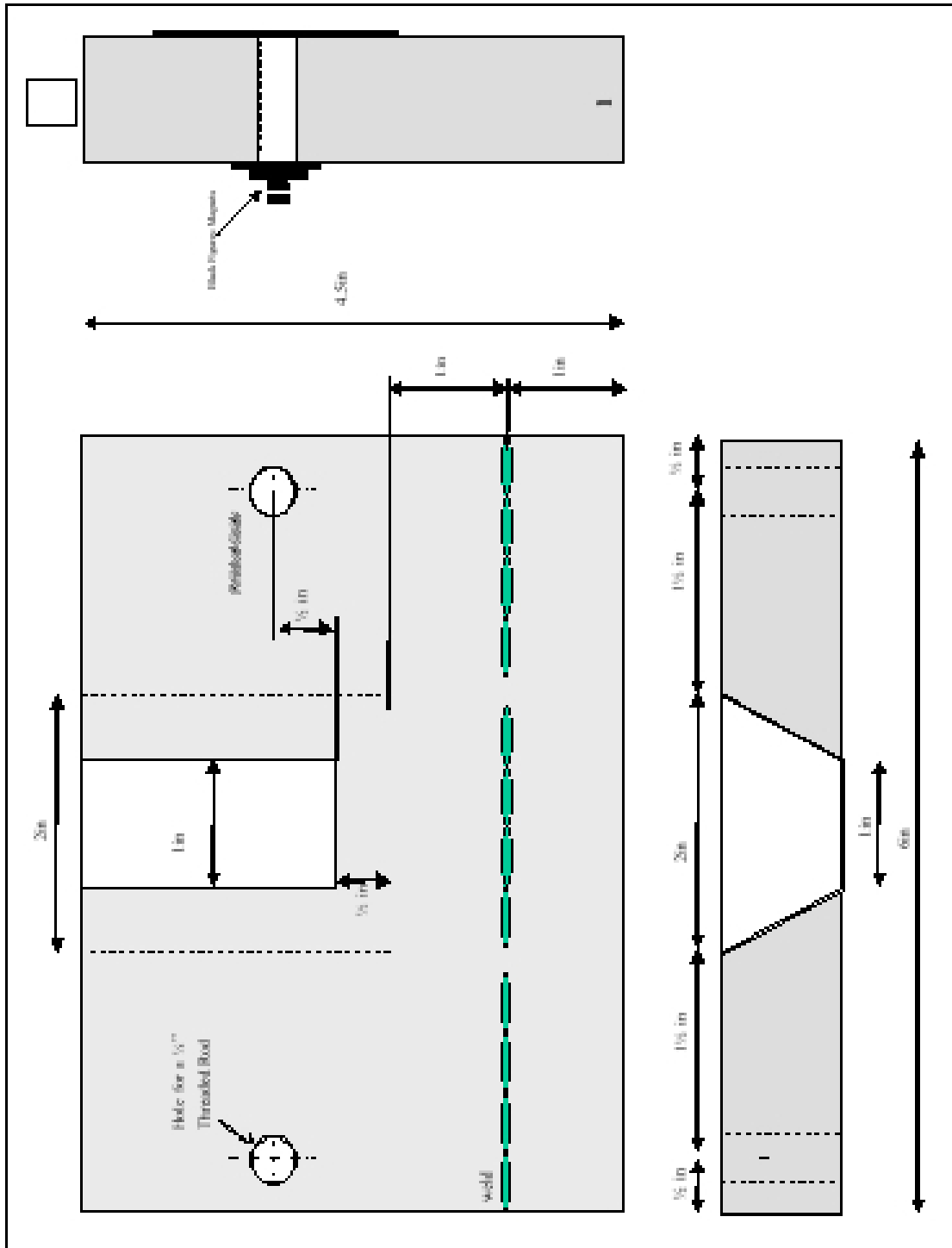Figure 9. Engineering diagram of the magnetic set-up frame.

18

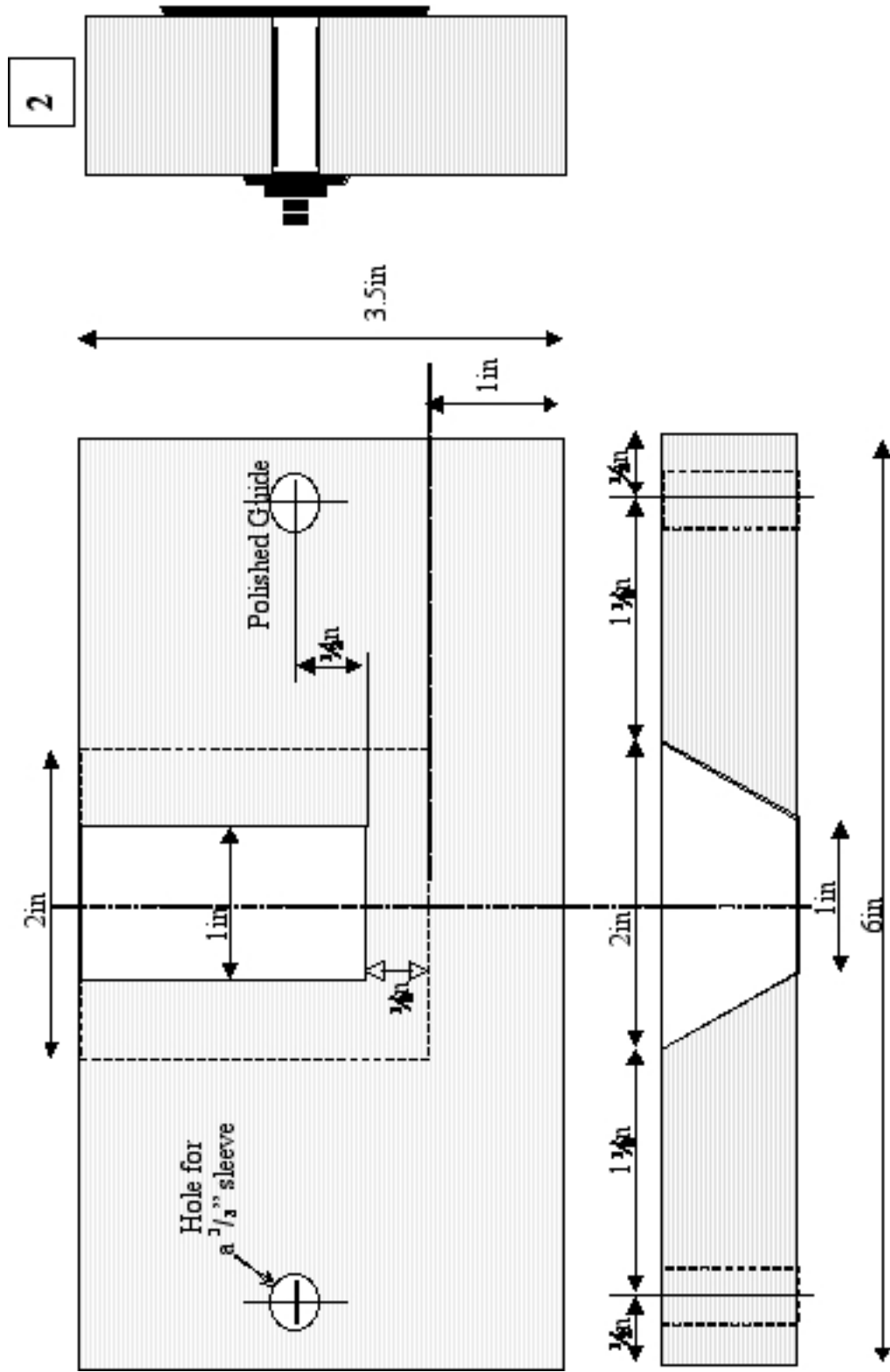Figure 10. Engineering diagram of fixed aluminum sheet No. 1 from Figure 8.

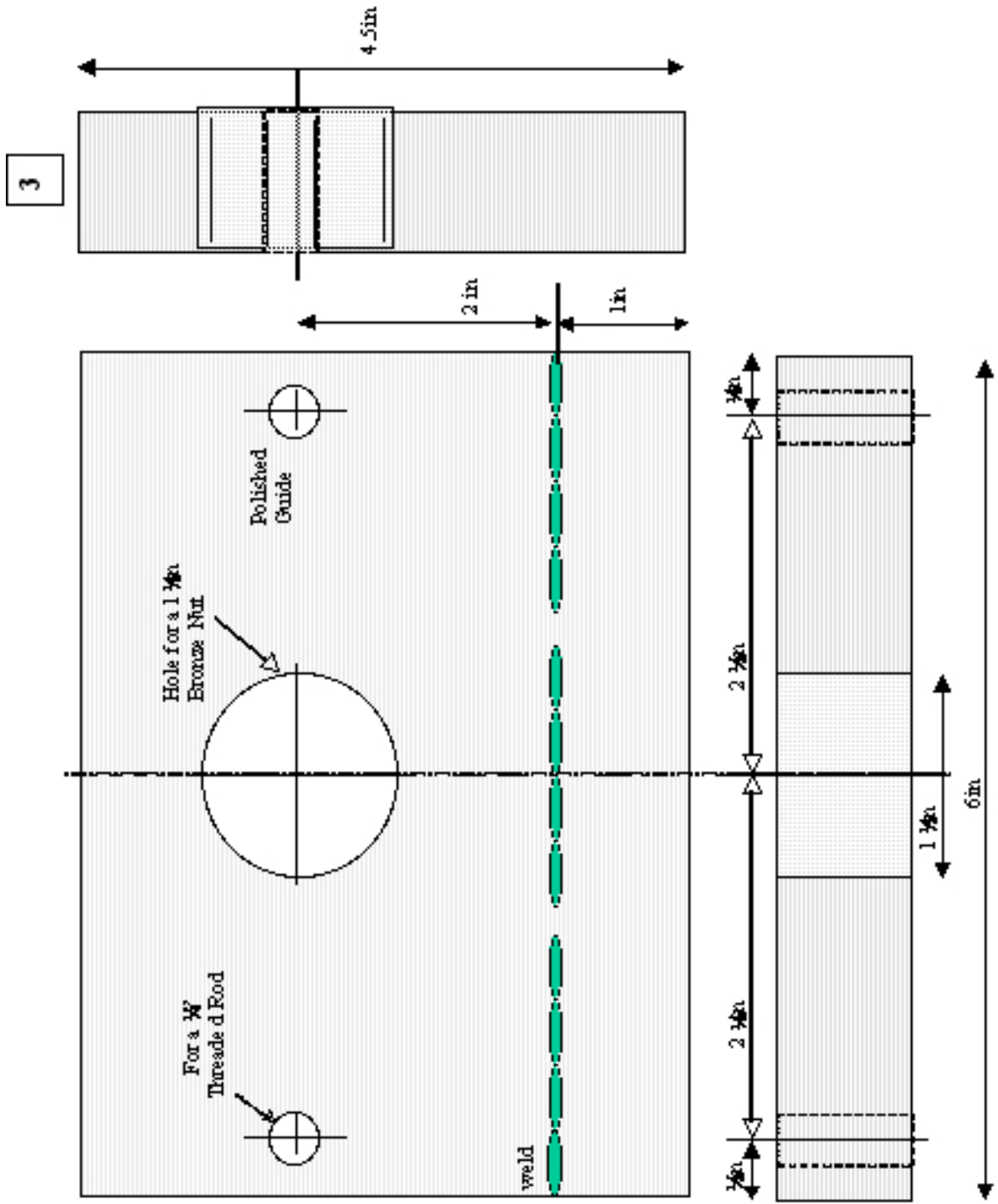Figure 11. Engineering diagram of traveling aluminum sheet No. 2 from Figure 8.

Figure 12. Engineering diagram of fixed aluminum sheet No. 3 from Figure 8.
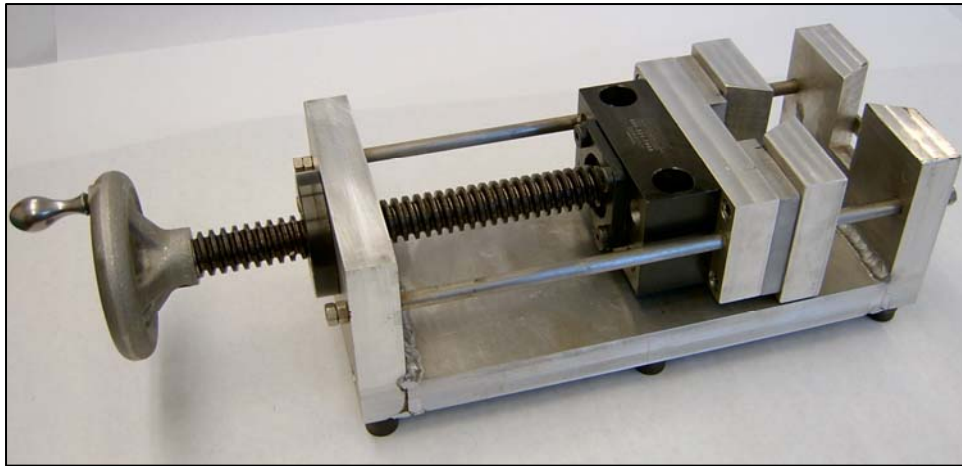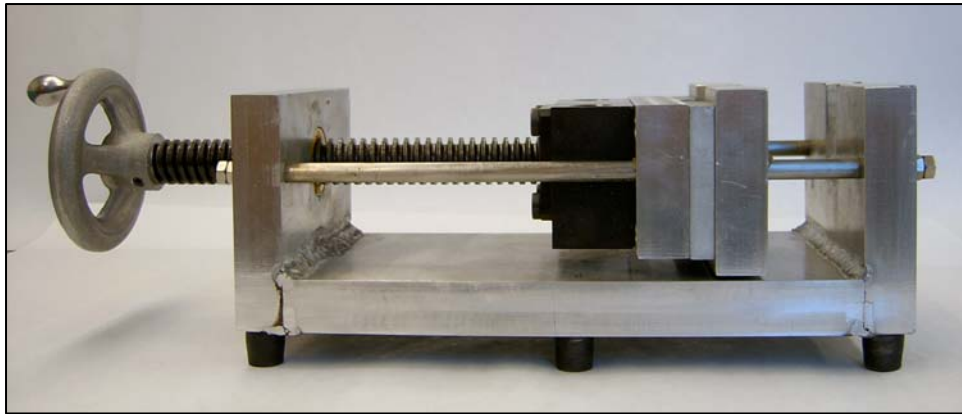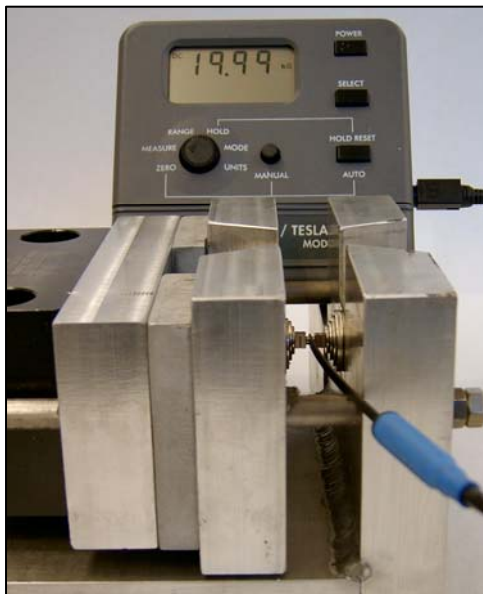
Figure 13. Magnetic-Setup Frame.

Figure 14. The recorded magnetic induction value placing the Gauss meter sensor is placed between the steel sample and the permanent magnets. The magnetic flux density obtained exceeds the Gauss meter range: 2 Tesla (20 Kilo-Gauss).

d.　Hydrogen Cathodic Charging

The determination of the diffusion or mobile hydrogen concentration in pipeline steels is possible using the electrochemical techniques called Barnacle electrode, which is based on the standard test method ASTM F-1113. This method essentially makes use of the extraction side of the Devanathan-Stachurski cell and requires that the samples have being previously charged with a uniform known distribution of hydrogen throughout. Unexpectedly, this initial hydrogen charging experiment and the thermodynamic approach brought to the light the fact that the hydrogen concentration can be calculated without and with an applied magnetic field. This approach will demonstrate rapidly the baseline of the Equation 10, which says that the hydrogen solubility will increase exponentially with increasing magnetic flux density.

To determine hydrogen concentration in a steel sample after a hydrogen charging experiment the LECO-Hydrogen Determinator RH-404 is used. Because this elemental analyzer requires a 1 g-sample, several 0.35x1.0 in (8.89x25.4 mm) parallelepiped-shape specimens are sectioned from the selected steels API 5L X52, X70, and X80. One group of samples is employed for the hydrogen charging experiment without an applied magnetic field and the second group for the experiment run under a strong, uniform magnetic flux density. All the specimens are subsequently cleaned in non-chlorinated solvents, rinsed with acetone for five min, and baked at 400ºC for one hour to remove any remain hydrogen from manufacturing.

For the first experiment, the samples are mounted on epoxy resin. The epoxy resin reduces the galvanic cell effect in the Hydrogen-Charging System and ensures complete submerging of charged area into the solution. The uncharged hydrogen concentration was determined with a three-specimen set using the LECO-Hydrogen Determinator RH-404. The other mounted-specimen set is electrically connected to a copper wire and surface finished until a common bench grinding finish was obtained. The sample is submerged into the charging solution as shown in Figure 15.

For the magnetization experiment, the samples are placed between two sets of permanent magnets as is explained widely in both sections Magnetic Flux Density and Magnetic-Setup Frame. The sample-magnet assembly is lately submerged into the charging solution (Fig. 16). To avoid any attraction among the magnets, a plastic frame is placed between them. The charging solution is prepared using analytical reagents and commercial pure distilled water. Even tough the massive magnets are not electrically in contact with the sample (anode), some bubbles are produced on magnets surface due to, basically, acidity (pH ~ 0.4) of the charging solution.
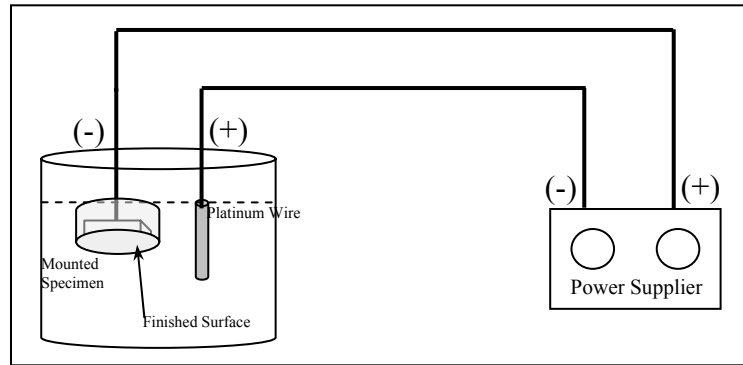
Figure 15. Schematic diagram of hydrogen cathodic charging apparatus for the experiment without a magnetic field applied to the sample.
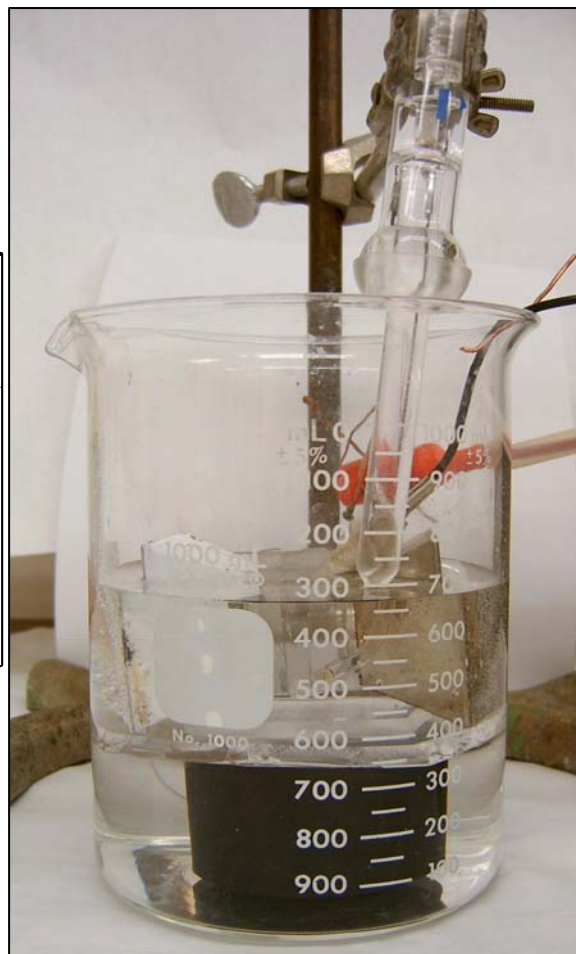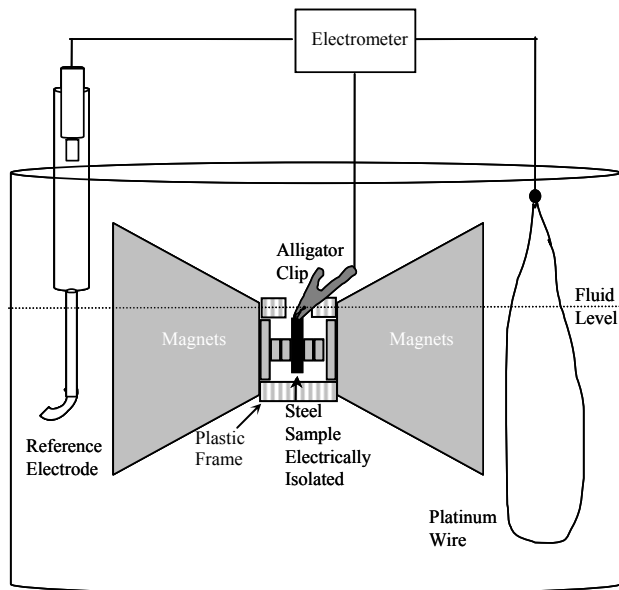

Figure 16. Magnet-sample setup submerged in charging solution (1N H_2SO_4)

The cathodic charging is carried out electrolytically in a fresh-500 ml solution of 1N H_2SO_4, using a platinum wire as cathode and the steel sample as the anode. The temperature (T_{room}) and pH (up to 0.4 at t = 0) of the solution were continuously monitored. The test is performed and the experiment parameters are controlled electronically using a potentiostatic/galvanostatic unit (EG&G PARC model 273A) and the commercial measurement software 352 SoftCorr III (Figures 17 and 18). With the purpose of establishing the required potential to promote hydrogen-atom oxidation reaction, a polarization curve is obtained (Fig. 19). This experimental curve shows that the hydrogen charging experiment must be run at a potential greater than 500 mV to ensure hydrogen dissociation. Consequently, the current rate is fixed at 0.05 A/cm^2.

The exposed area of each specimen is monitored and recorded in the corrosion software setup files. The achieved hydrogen concentration values are plotted as a function of time with the purpose of distinguishing the effect of the magnetic flux density. The charging time is fixed in intervals of 1, 2, 3, 6, 8 and 12 hours to establish the equilibrium hydrogen concentration. That is, the plateau of hydrogen concentration curve which represent the equilibrium point. Previous and convincing results on magnetization effect have already been obtained for the X52 steel (see Progress Results section).

Figure 17. Potentiostatic/Galvanostatic Unit
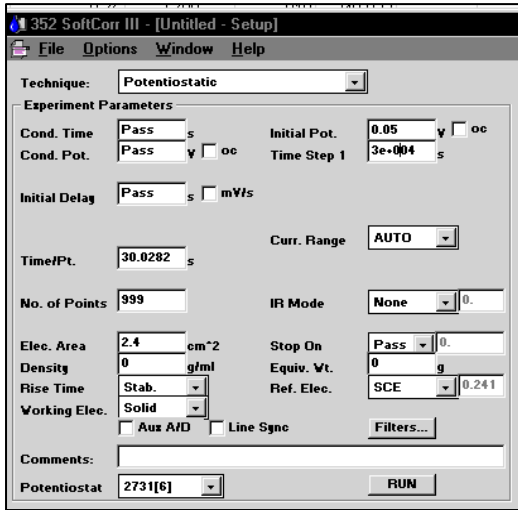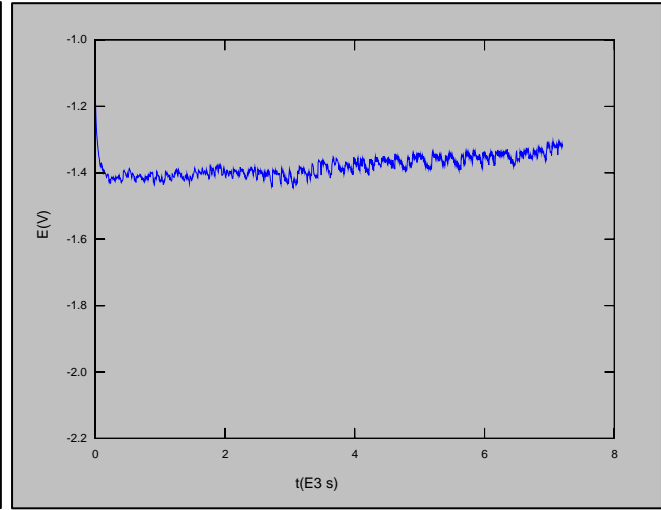
(a)   (b)

Figure 18. Windows of commercial corrosion software: 352 SoftCorr III.
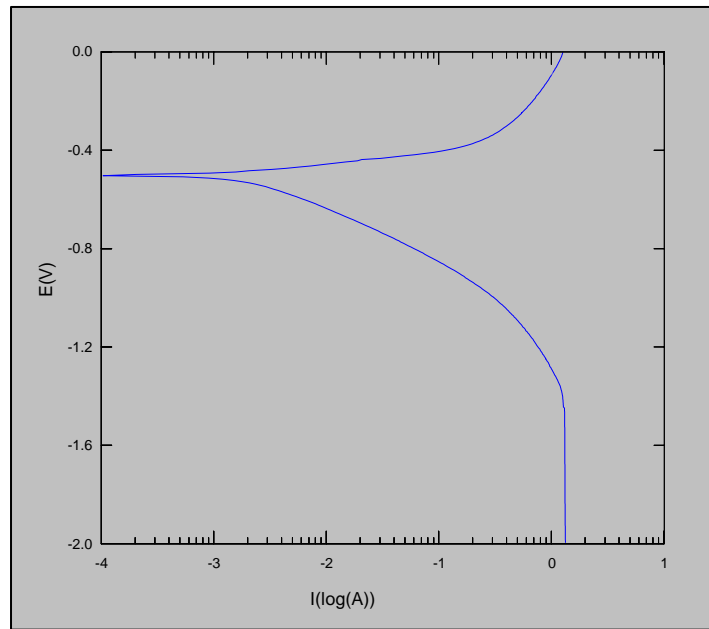(a) Setup data and (b) Potential-time plot.

Figure 19. Polarization Curve of steel Grade X52
(Software: 352 SoftCorr III).

e.   HYDROGEN CONTENT DETERMINATION

Once steel samples are hydrogen-charged hydrogen content is measured using
the LECO Hydrogen Determinator RH-404 (Fig. 20). This determinator
utilizes the inert-gas fusion technique to measure specifically the hydrogen
concentration in inorganic materials. These materials, such as steel, require
high-temperature fusions to effectively releases hydrogen. In other words, the
determinator melts steel-specimen releasing hydrogen gas, which is
determined by thermal-conductivity difference.

(a) Measurement Unit   (b) Furnace

Figure 20. Photograph of LECO RH-404 Hydrogen Determinator. Standard
1gr-5.8ppm samples are used before pipeline steel experiments to ensure
calibration. The monitor display shows hydrogen content of a standard steel
sample: 5.78 ppm of hydrogen.

Measurement and furnace units constitute the LECO Hydrogen Determinator
RH-404. The weight and physical dimension of a steel sample used in it is
limited. The normal specimen weight range is 0.5-1.0 grams while the
maximum diameter is 7.5 mm (0.295 in) and the maximum length is 18 mm
(0.708 in).

Consequently, to satisfy these limitations, the pipeline steel specimens are
sectioned in small pieces, which are hydrogen-charged before hydrogen
content detection. In fact, the weight of steel samples is roughly 1gr while the
physical dimensions are approximately 4 mm x 5 mm x 10 mm (0.157 in x
0.197 in x 0.394 in); that is, wide x height x length.

With the purpose of calibrating the LECO Hydrogen Determinator RH-404, three steel standard 5.8 ±0.4 ppm-samples are used before any pipeline steel (X52, X70, and X80) sample is dropped into the electrode furnace. Figure 16 shows the calibration point before the hydrogen content was determined for a six hour charging steel X52-sample under a magnetic flux density of 2 Tesla (20,000 Gauss).

f.   Electrochemical Techniques

The assessment of magnetization effects on hydrogen damage of pipeline steels starts with the measurement of the absorbed-hydrogen concentration with and without magnetic flux density after several periods of charging time. This set of cathodic charging experiments brings to light the fact that the hydrogen concentration is affected by the magnetic flux density without differentiating this effect either on hydrogen diffusion or hydrogen solubility. Consequently, an electrochemical technique would be used to determine the effect of magnetic flux density on the permeation rate of electrolytic hydrogen. To experimentally perform this technique the Devanathan-Stachurski cell covered by the standard practice ASTM G148 would be used, respectively. Based on previous investigations concerning hydrogen permeation rate and mobile hydrogen concentration, the critical experimental parameters of each technique are defined and subsequently analyzed.

Based on the theory that the rate of permeation of hydrogen is controlled by diffusion in the material, the Devanathan-Stachurski electrochemical cell measures the instantaneous rate of permeation of electrolytic hydrogen through membranes of materials. This technique is used to evaluate the severity of hydrogen charging produced by diverse sources (corrosive environments and cathodic polarization) and to determine the effect of processing, metallurgical, and environmental variables, as well as properties of materials on diffusion of hydrogen in metals.

Basically, the Devanathan-Stachurski cell utilizes a metallic membrane forming the partition wall between two compartments of a twin electrochemical cell with electrodes in each one. One side of the membrane (charging side) is coverage with absorbed atomic hydrogen produced by cathodic reduction at a certain fixed level, while on the opposite oxidation side the amount of atomic hydrogen should be always zero.

The charging cell contains an acid solution while the oxidation cell contains an alkaline electrolyte. The first promotes hydrogen charging while in the second the membrane surface is kept passive at a potential, high enough to oxidize by anodic polarization (potentiostatic circuit) any hydrogen coming through the membrane. The current in the anodic potentiostatic circuit obeys

the Faraday's laws measuring the instantaneous rate of permeation of hydrogen.

In other words, in the charging or cathodic electrochemical unit the hydrogen evolution reaction is produced. Applying a fixed and constant current to the specimen surface the reaction takes place. While the anodic or oxidation electrochemical unit is where the hydrogen atoms arrive and are oxidized after permeating through the membrane.

g.   Devanathan-Stachurski Permeation Cell

i   Apparatus

The Devanathan-Stachurski cell (Fig. 21) consists of two identical electrochemical units, charging and oxidation, terminating in standard ½ in (12.7 mm) pipe flanges. Each flange holds a Teflon O-ring facing the refined and flat membrane. The assembly is jointed with the membrane in between the O-rings. The electrode in the charging compartment is bright platinum auxiliary and the electrodes in the oxidation cell are a bright platinum auxiliary and Lugging capillary-calomel reference.
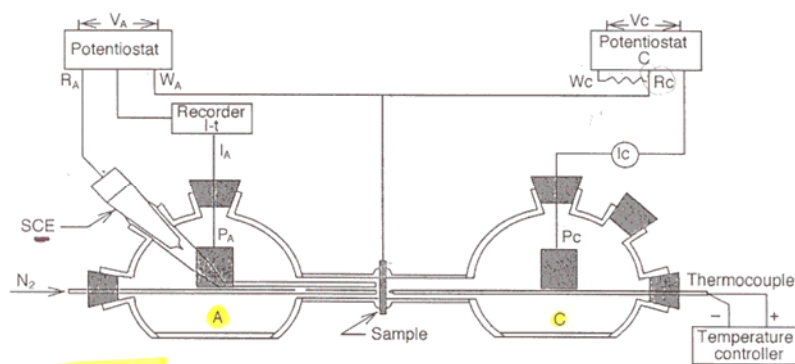
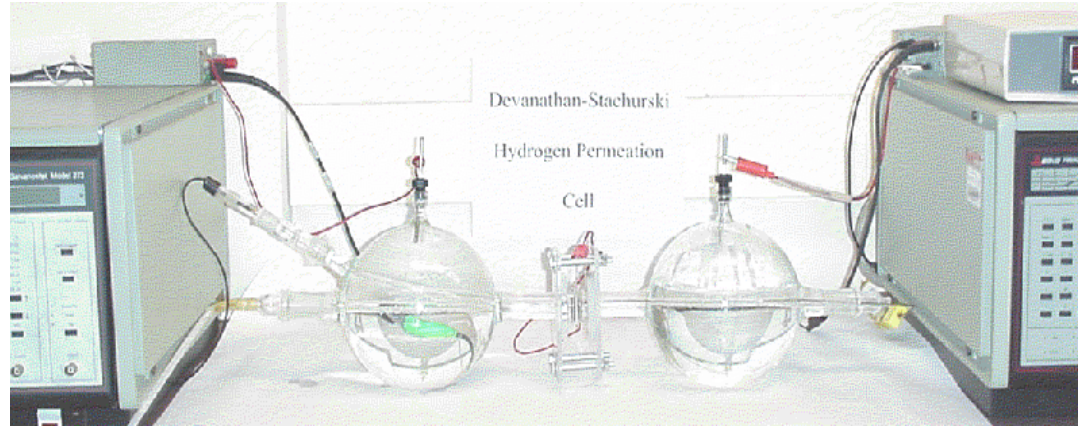Schematic Diagram (Yen, S.K., et al.)

Figure 21.   Hydrogen permeation cell (Devanathan-Stachurski) and schematic diagram. C: cathodic unit. A: anodic unit. P_C-P_A: auxiliary platinum electrodes. R_C-R_A: reference P_C electrodes. W_C-W_A: working electrodes.

The charging or cathodic unit is filled in with 1.3 liters of an acid solution, and a constant current density of 50 mA/cm^2 (500 A/m^2) was applied to the cathodic surface of the specimen. The anodic unit is filled in with 1.3 liters of a solution of 0.1N sodium hydroxide and potentiostatically maintained at 50mV$_{SCE}$. It is applied to the anodic surface of the specimen to force the hydrogen concentration on the surface to zero. Both solutions are previously deaerated by pure argon 30min. right before the test. Pure argon is injected into the outlet compartment to promote storing. A palladium coating, commercially known as Pallamerse, is applied on the exit surface of the membrane to moreover ensure zero hydrogen concentration and on the charging side to protect. Enhanced efficiency of the hydrogen atom oxidation reaction is reached once the anodic surface is coated (palladium). It means palladium-coating serves as a catalyst for the following reaction

$$H° \rightarrow H^+ + e^-$$

[12]

The test is performed and the experiment parameters are controlled electronically using two EG&G PARC model 273A potentiostatic/galvanostatic units. Commercial computer software is utilized to record the oxidation current.

30

ii   Test Environment

The test environment is designed to facilitate ease and reliability of
making hydrogen permeation measurements. Because the laboratory
environment is prepared using analytical grade reagents a pre-electrolysis
treatment will no be used. Commercial pure distilled water is also utilized
to prepare the environment. The volume of solution to metal area ratio is
up to 550 ml/cm^2.

For the reason that pH and temperature of the solutions have a significant
effect on hydrogen permeation, both parameters are continuously
monitored. The experiments are carried out at room temperature and a
constant pH. Any variation is recorded. The charging cell is
thermostatically controlled at room temperature for the period of the
experiment.

Chemical Solutions

From previous works, the initial acid solution to fill in the cathodic cell
was 0.2N acetic acid (CH_3COOH) - 0.1N sodium acetate ($CH_3COOHNa$)
solution. However, preliminary experiments cause a low rate of reaction
between the solution and the steel sample. Because the charging or
cathodic solution strongly affects the hydrogen permeation rate, it
represents a critical parameter of the Devanathan-Stachurski technique.
Consequently, any variation from its original selection would be
straightforwardly accepted if preliminary results identify it as an uncertain
parameter. Hereinafter, the new cathodic solution is:

➢ *1N H_2SO_4*

   1M = mass/L / GFW (gram formula weight)
   1N = 1M * Z
   Acid: Z is the number of hydroxide ions liberated
   1M = mass/L / (98) = mass/L / 98
   1N = 1M * Z (sulfuric acid=2) = mass/L / 49
   Concentration: 49 gr./L (1N)
   Liquid Solution Density: 1.84 gr/cc.
   Final Concentration *1N H_2SO_4* = 49 / 1.84 = 26.6 cc/L

In contrast, the alkaline anodic solution to fill in the anodic cell is 0.1N
sodium hydroxide. This oxidation solution would not be modify due to the
slightly effect on measurements. The calculations are the following:

> *0.1N NaOH*

    1M = mass/L / (23+16+1) = mass/L / 40
    1N = 1M * Z (=1) = mass/L / 40
    Concentration: 40 gr./L = 1N
    0.1N = 0.1 * 1N
    Concentration *0.1M NaOH* = 4gr/L

iii *Specimens*

Specimen characteristics are critical parameter to determine hydrogen permeability rate. The preliminary specimens used in this study are 1.60 mm (0.063 in) thick, 1 in^2 (645.16 mm^2) total area, flat, and surface grinding finished. However, since thickness, total area, and surface finish have a significant effect on hydrogen permeation experiment, these parameters would be considerably modified if needed. Thicker samples increase experiment timing, small specimens affect electrical contact area, and surface finish at oxidation side affects hydrogen extraction.

Mechanical cutting is the selected manufacture method to machine the specimens because electrochemical discharge machining may introduce hydrogen into the metal modifying the initial concentration. Although, the initial selected surface finish is the given by a common surface grinder, it would be up to #600 grit at both charging and oxidation side. As propose of this study, both surfaces are similarly treated in order to experimentally demonstrate the principal subject of this work. The theoretical relation between hydrogen concentration and magnetic field does not obey any service condition modeling.

After polishing, the specimens are cleaned in non-chlorinated solvents for five min. to removes traces of chemicals and degreased before experiment and then rinse with acetone for five min. Finally, it is dried by warm air blowing just right before the electrochemical cell assembly.

Although it is well know that a palladium coating on the charging face of the specimen affect the sub-surface hydrogen concentration, a thin palladium coating is applied. This suitable material *"can minimize variations in surface conditions during the permeation transient and yield repeatable transients provided the specimen thickness is adequate"* (ASTM G148, 1997).

iv *Test Procedure*

Based on ASTM G148-97 "Standard Practice for Evaluation of Hydrogen Uptake, Permeation, and transport in Metals by an Electrochemical Technique."

The deaeration begins by active purging on immediately addition of the solution to the charging cell. It rapidly removes oxygen that may contaminate the solution and affect the environment concentration and specimen surface.

The commercial software M365 SoftCorr III from Princeton Applied Technology is used to monitor the total oxidation current as a function of time. The experiment run until the anodic current achieves steady-state condition. The preliminary test results will permit to refine all experimental parameter.

v *Environmental Control and Monitoring*

Based on ASTM G148-97 "Standard Practice for Evaluation of Hydrogen Uptake, Permeation, and transport in Metals by an Electrochemical Technique."

vi *Procedures for Analysis of Results*

Based on ASTM G148-97 "Standard Practice for Evaluation of Hydrogen Uptake, Permeation, and transport in Metals by an Electrochemical Technique."

When the instantaneous rate of hydrogen permeation is recorded, the hydrogen diffusion coefficient can be calculated by a variety of methods (Devanathan and Stachurski, 1962). As propose of this study, the time lag method, the breakthrough time method, and the rise time method are considered.

vii *Reporting.*

Based on ASTM G148-97 "Standard Practice for Evaluation of Hydrogen Uptake, Permeation, and transport in Metals by an Electrochemical Technique." In addition, a record of the diffusion coefficient values plotting D_{eff} as a function of the magnetic field is required.

h. RESIDUAL STRESS

Although it is widely known that cold work increase hydrogen absorption in low-carbon steels, the effect of high magnetic flux density on hydrogen intake in cold-worked high strength steels is undetermined to date. To assess this phenomenon, conventional small specimens alike those used in hydrogen charging tests are sectioned from cold-worked steel samples.

Pipeline steel samples are loaded to various levels of bending stresses and the effect of the residual stresses under a magnetic induction on hydrogen absorption is measured. To achieve comparable results, the experiment is run under same characteristic of the hydrogen-charging test.

Tensile test specimens and method from API Specification 5L are used to obtain the charging samples, which are classified into two categories: "samples without magnetic field" and "samples with magnetic flux." Are loaded up to both determine the mechanical properties of the steel and reach different elongation levels. Table 3 describes the purpose of each tensile test specimen.

Hydrogen-charging samples are sectioned from the cold-worked tensile test samples loaded at different elongations. Absorbed hydrogen concentration at several charging times is measured and plotted. The effect of cold-work on hydrogen absorption in pipeline steels will be shown in the chart.

Table 3. Number and purpose of the Tensile Test Specimens

Pipeline Steel Grade	Tensile Test Specimen	Purpose of Test
X-52	1 2 3 4 5	Verification of Mechanical Properties " 5% Elongation 10% Elongation 15% Elongation
X-70	1 2 3 4 5	Verification of Mechanical Properties " 5% Elongation 10% Elongation 15% Elongation
X-80	1 2 3 4 5	Verification of Mechanical Properties " 5% Elongation 10% Elongation 15% Elongation

5. PROGRESS RESULTS

With the purpose of demonstrating the effect of a strong, continuous magnetic field on absorbed hydrogen content in pipeline steels, thirteen (13) steel grade X-52 samples were cathodically tested. That is, eight specimens under a non-magnetic field and five (5) under a 2 Tesla (20,000 Gauss) magnetic induction. The absorbed hydrogen concentration at different cathodic charging time was plotted in the chart shown in Figure 22.

Even though a final project conclusion would not be obtained from this chart, these plotted points lead to an important tendency. In other words, a strong and continuous magnetic field causes a tremendous effect on absorbed hydrogen concentration in pipeline steel grade X52. After reaching the saturation level (plateau), the hydrogen content in steel samples under a 2 Tesla magnetic induction is approximately eight (8) times the concentration under cathodic charging conditions without an applied magnetic field. This remarkable, observed effect becomes one of the primary proposes of this project. According to Figure 22, the saturation point of pipeline steel grade X52 is reached approximately after four (4) hours of cathodic charging in 1N sulfuric acid (H_2SO_4).

6. EARLY INTERPRETATION

Based on Equation 16 and Figure 22, the equilibrium point of absorbed hydrogen concentration under initial experimental conditions (without magnetization, B=0) is represented by $[H]_{B=0}$, i.e. ln $[H]_{B=0}$. This point is reached at plateau level; that is, $[H]_{B=0}$=1.29ppm (ln $[H]_{B=0}$= 0.2231). On the other hand, the plateau level of the magnetic flux density curve represents the absorbed hydrogen concentration at the specific magnetic induction of 2 Tesla (20,000 gauss). In other words, [H]=7.9ppm and the Equation 16 becomes:

$$Ln[H]_{B=B} = Ln[H]_{B=0} + \left(\frac{\Delta M}{2RT}\right)B \qquad [16]$$

$$Ln[7.9\,ppm] = Ln[1.29\,ppm] + \left[\frac{\Delta M}{2RT}\right] * 20,000G$$

It is well known that the slope of this straight line, $\Delta M/2RT$, is a property of the assessed pipeline steel under the experimental conditions. In other words, different pipeline steels generate different straight-line slopes. Steel grade X52 produced a slope of 0.0001 (Fig. 23). It is expected that steels X70 and X80 produce a greater slope because of their higher-strength characteristics and microstructures.
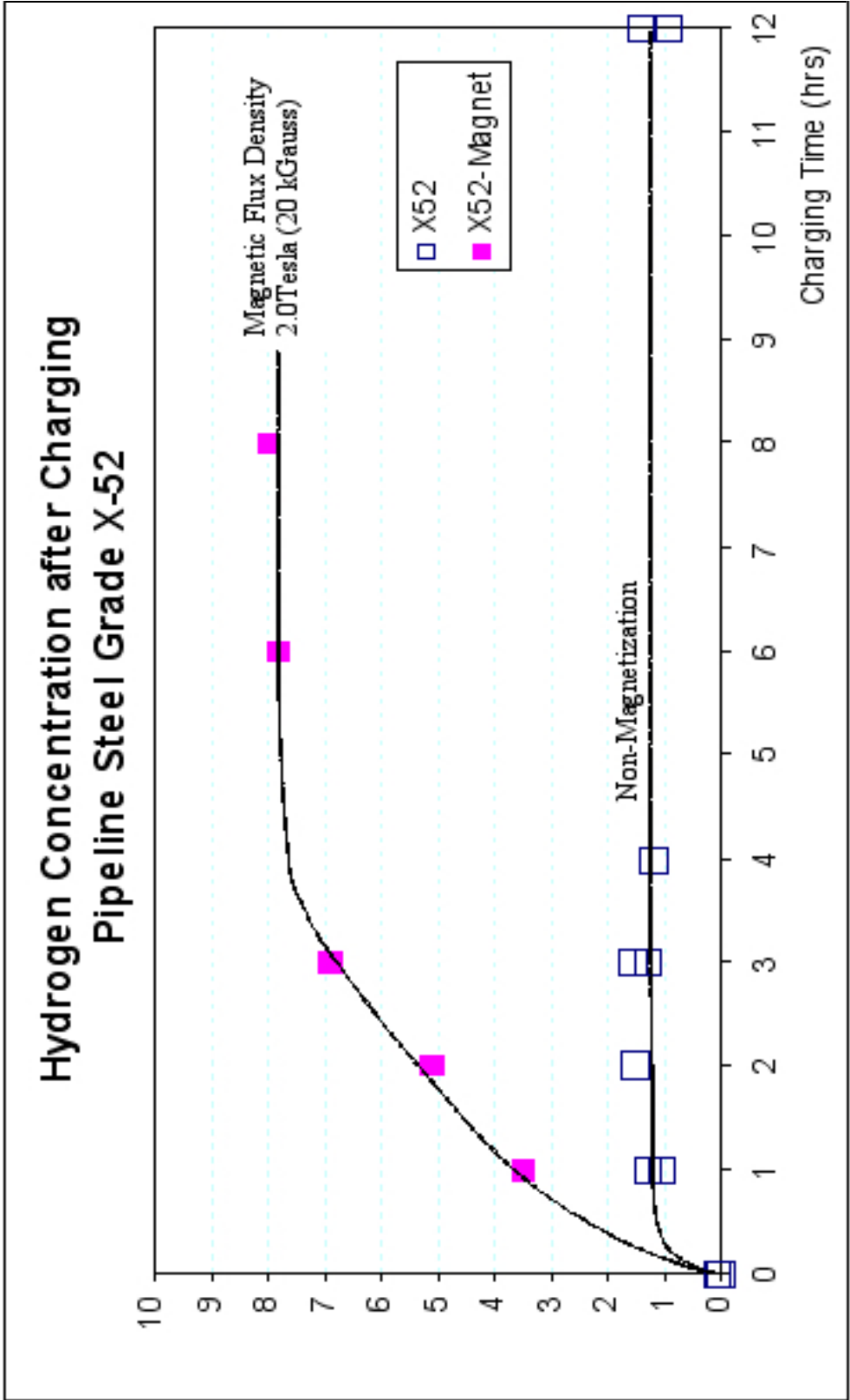
Figure 22. Absorbed hydrogen concentration in pipeline steel grade X52 at different cathodic charging time, showing the experiment result without magnetization and under a 2 Tesla (20,000 Gauss) magnetic induction.
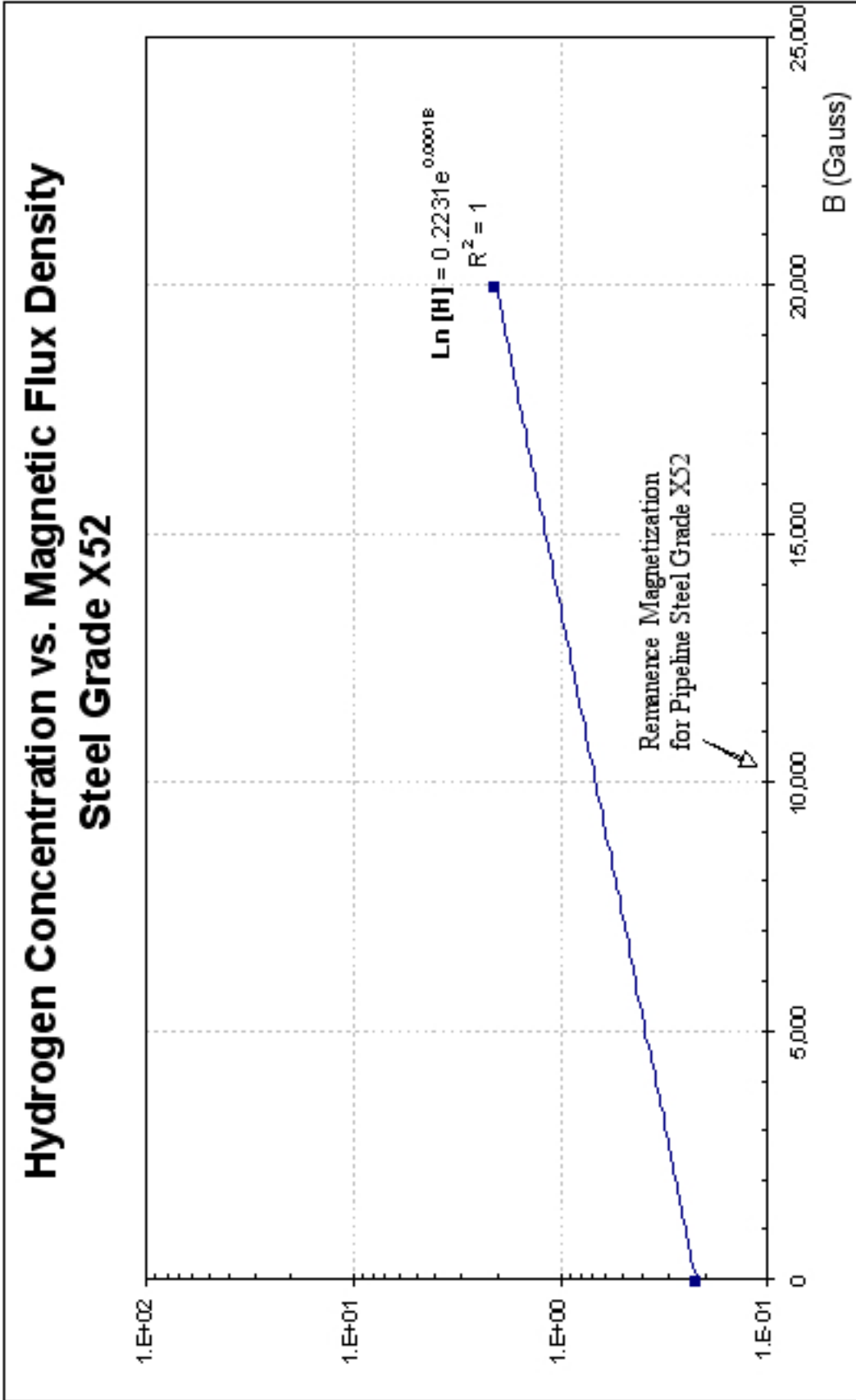
Figure 23. Graphical representation of Equation 16.

Figure 23 illustrates the graphical expression of the experiment using the experimental data from Table 4.

Table 4. Experimental data from Figure 22.

Parameter	Experimental Conditions	
	Without Magnetization	Magnetization
Equilibrium Hydrogen Concentration $[H]_{B=0}$ (ppm)	1.250	--
ln $[H]_{B=0}$	0.223144	--
Hydrogen Concentration $[H]$ (ppm)	--	7.9
ln $[H]$	--	2.067
Magnetic Flux Density (Gauss)	0	20,000

The ln[H]/ln[H]$_{B=0}$ratio equal to 9.3 leads to the following statement: '*a magnetic induction of 20,000G increases in more than nine times the absorbed hydrogen concentration of pipeline steel grade X52.*' It brings to the light an important question: *how much the absorbed hydrogen content increase under the remaining magnetization left by the Magnetic Flux Leakage tool after inspection operations?*

This fundamental question can be responded by the analysis of in-between points of the straight line from Figure 23. In other words, if the remanence magnetic induction (Br) in the steel grade X52 is 10,000G, therefore the potential absorbed hydrogen content increases approximately three times (Table 5). However, this is possible if either the magnetization is constant or there is not a surface anomaly that can increase the magnetic induction over it. Surface anomalies such as cracks (at crack tip) and dents increase considerably the magnetic flux density within the magnetic flux leakage process. It can reach magnetization level greater than the

remanence, thus the potential absorbed hydrogen concentration under these conditions would increase even more than three times.

Table 5. Determination of in-between points.

In-between Points	
Magnetic Flux Density B	10,000
Ln [H]	0.606
Ln[H] / Ln[H]$_{B=0}$Ratio	2.718

7.   FUTURE WORK

To assess the magnetization effect on hydrogen cracking for thick walled steel pipelines four variables where previously defined. These variables are pipeline steel grade, wall thickness, residual stress effect, and magnetic flux density. Subsequent experiments will include:

➢ Cathodic charging of pipeline steel grade X70 and X80 under both experimental conditions without and with magnetic induction.

➢ Vary the magnetic flux density to 10,000G and determine the plateau level for the three steel grades to confirm the early interpretation.

➢ Assess the cold-work effect under same experimental conditions using the steel-grade samples already described in residual stress section.

➢ Assess the magnetization effect on mechanical properties of steels using the conventional NACE standard test methods or a combined set of tests utilizing both conventional standards and newly designed procedures.

APPENDIX A

REPORT

Thermoelectric Power Coefficient Assessment of Hydrogen in Pipeline Steels

1.   ABSTRACT

The preliminary investigation was performed to measure and monitor the diffusible hydrogen content using rapid electronic property measurement technique. To measure the hydrogen content in pipeline steel, low temperature thermoelectric power (TEP) measurement was used for hydrogen charged HSLA steel samples. The measurement of as-received HSLA steel sample shows a negative slope and decreases with time within two minutes as the specimen warms up from liquid nitrogen temperature to room temperature. The thermoelectric power coefficient of the corresponding hydrogen-charged specimen increases with time as it warms up from liquid nitrogen to room temperature. The large difference in the thermoelectric power coefficient at the low temperature range (about -140 ^{o}C) between uncharged and charged specimens was observed. This result indicates that the thermoelectric power coefficient can be amplified at low temperatures, resulting in accurate measurement in the thermoelectric power coefficient for the hydrogen-charged HSLA steel. Also, the TEP coefficient measurement of HSLA steel welded with hydrogen containing shielding gas was performed as a function of specimen temperature and time. The instantaneous amounts of diffusible hydrogen for weld metal can be obtained by recording both the TEP coefficient value and specimen temperature for diffusible hydrogen measurement practice. The TEP coefficients of fixed sample temperature, such as -60 and -40 ^{o}C, show linear relationship with different diffusible hydrogen content as a function of diffusible hydrogen content. In addition, the TEP coefficient measurement results as a function of time results can be used to curve fit a standard plot to determine the resulting diffusible hydrogen content for steel weld metal by using the error function. These preliminary experimental results show potential use of TEP coefficient measurement technique to assess the hydrogen content in pipeline steel.

2.   INTRODUCTION

Through the utilization of modern physics concepts, a portable non-destructive thermoelectric power device has been designed for determination of hydrogen content in HSLA steels. The thermoelectric power coefficient is extremely sensitive to microstructural changes, and with careful correlation to standards it can be used as a rapid, non-destructive technique to assess the alloy composition and microstructural variations before potential loss of integrity in the HSLA steel

specimen. The HSLA steel specimens have been charged to various hydrogen contents and then the thermoelectric power coefficient monitors the change in hydrogen content with time as the hydrogen diffuses out of the HSLA steel specimen. Different conditions in the thermoelectric power measurement procedure were investigated to determine if increased sensitivity could be achieved in by making measurements at liquid nitrogen temperature relative to room temperature. This practice was performed since we know that low temperature TEP measurements are much more sensitive.

The second effort of this study was devoted to measure TEP coefficient at low temperature to measure the diffusible hydrogen content for ferritic or martensitic steel welds. The TEP coefficient was measured as a function of time and temperature for different diffusible hydrogen content in HSLA steel welds. The TEP coefficient measured as a function of time can be used to find the initial hydrogen content using the error function. It is very important to notice that there is a large TEP coefficient at low temperature and much smaller coefficient at the room temperature range. This result indicates that TEP signal could be amplified at low temperature.

This report consists of three sections: theory section, preliminary experiments section, cryogenic Seebeck measurement section, and dynamic Seebeck measurement section.

3. **THEORY**

The thermoelectric power coefficient is a function of the electron concentration, the effective mass of the electrons, the electronic scattering behavior in an alloy, which are all influenced by the solute content, lattice strain, microstructural changes, material processing, and time-dependent phase changes. In metallic alloys, the value and the sign of the thermoelectric power coefficient are dependent upon the electronic features in the vicinity of the Fermi energy level, the effective mass tensor, the density of electronic states, and the dominating scattering mechanism [1]. In turn, the Fermi energy value (Fermi energy surface in the k-space) changes with electronic filling in the conduction band due to the electron donation by hydrogen atoms. For example, with the high degeneracy of the free electron gas, the resulting thermoelectric power coefficient, Z, is related to the electron theory through the following expression where the degeneracy of the electron gas is for high carrier concentrations:

$$ Z = \left(\pm \frac{\bar{k}}{e} \right) (27.1) \left(r + \frac{3}{2} \right) \left(\frac{m_e}{h^2} \right) \left(\bar{k} T n^{\left(-\frac{2}{3} \right)} \right) $$ [1]

where r is the scattering parameter determined by the dominating scattering mechanism, and h is Planck's constant, $\bar{\kappa}$ is Boltzmann's constant, n* is the

electron concentration, and m_e is the effective mass. From the free electron model, the electron concentration is directly related to the Fermi energy. The electronic effective mass defines the rate of Fermi energy change with increasing electron concentration [1]. The effective mass can be described as:

$$m_e = \hbar^2 \left(\frac{d^2 E}{dk^2} \right)^{-1}$$

[2]

where k is the wave number. The effective mass, m_e, describes the shape of the s, p, and d bands that are in contact with the Fermi energy level. The shape of the bands at the contact position offers a characteristic indication that can be measured with changes in the Fermi energy level due to electron donation from the hydrogen addition.

To observe thermoelectricity, it is necessary to have a circuit composed of two different materials, and the net difference between their thermoelectric properties can be measured. The electromotive force (emf) produced under these conditions is the relative Seebeck emf. The potential difference between the hot end and the cold end as illustrated at Figure 1. The developing voltage of each element is dependent upon the Seebeck coefficient difference between two metals Z_{AB}. The emf between the two metals, $V_{AB}=\Delta V_A-\Delta V_B$ can be expressed by:

$$V_{AB} = \int_{T_0}^{T_c} (Z_A - Z_B) dT = \int_{T_0}^{T_c} Z_{AB} dT$$

[3]

where $Z_{AB} = Z_A-Z_B$ is defined as thermoelectric power for the thermocouple A-B. The absolute Seebeck coefficient (ASC) of the alloy material, Z_a, can be determined from measurements as:

$$Z_a = \frac{V}{\Delta T} - Z_{Cu}$$

[4]

where V is the Seebeck voltage measured between alloy material and reference copper electrode, ΔT is the temperature difference, and Z_{Cu} is the well-calibrated Seebeck coefficient for copper. One copper probe is maintained at room temperature and the other one at a temperature higher by 10 °C. The temperature difference can be varied, but it must remain constant for all tests.
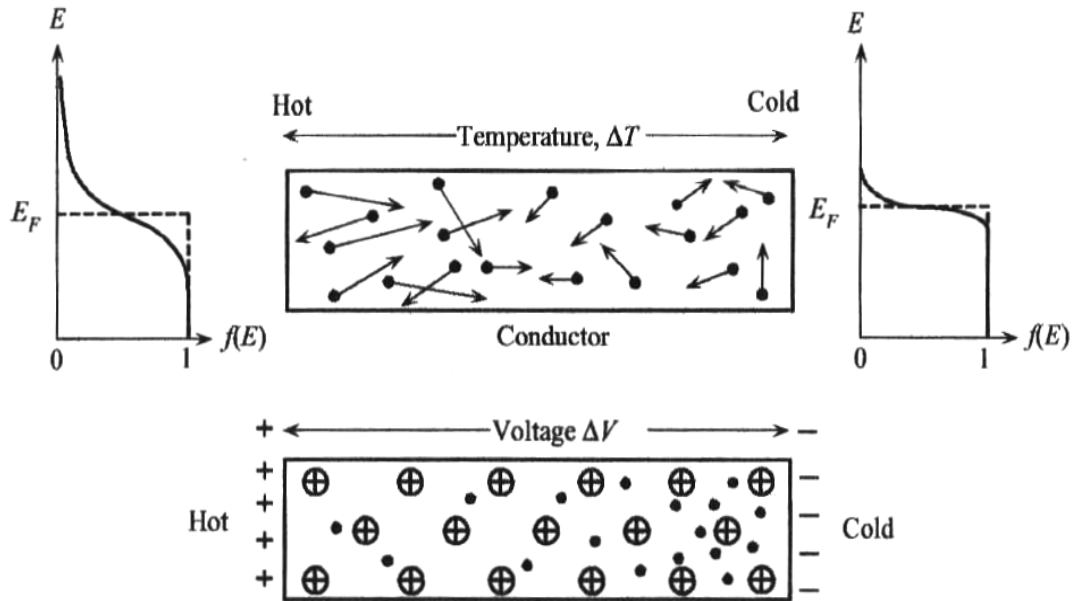
Figure 1. A temperature gradient (ΔT) gives rise to a potential difference
(ΔV), which is the Seebeck effect [2]. Free carriers in the picture are
electrons (N-type material).

4. PRELIMINARY EXPERIMENTS

Thermoelectric Power Coefficient Measurement Scheme

For the determination of hydrogen content using thermoelectric power, a non-destructive Seebeck measurement device has been developed.   The Seebeck apparatus consists of a Keithley Nano-voltmeter 2182, two Watlow temperature controllers and read-outs, two type T and two type K thermocouples, two heating cartridges, and two copper (or iron) reference probes. The thermoelectric power set-up used for hydrogen charged HSLA steel specimen consisted of two reference copper blocks (or iron) as shown in Figure 2(a). HSLA steels welded sample with hydrogen containing shielding gas is shown in Figure 2(b). A total of four different thermoelectric power measurement set-ups were used to maximize the measuring sensitivity.

Pure copper and iron are both used as reference materials in the thermoelectric power measurement set-up dependent upon the material being tested. The use of a pure iron reference is utilized to determine if there will be an increase in the resolution of the thermoelectric power measurement on HSLA steel specimens [3]. Copper has been used in most cases for thermoelectric power measurements because of its high thermal and electrical conductivity. It has been reported that

pure iron reference materials can increase thermoelectric power measurement sensitivity on HSLA steel specimens, which is due to the similarity in chemical composition.
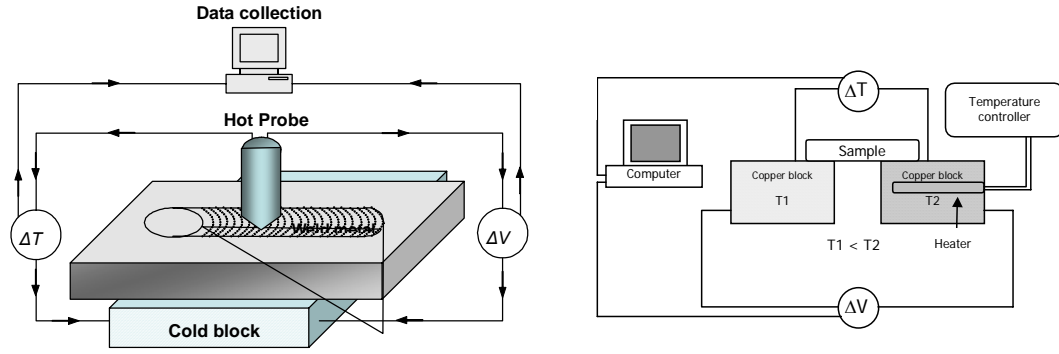

Figure 2. Schematic drawing of a) TEP measurement system used for hydrogen measurement of HSLA steel weldments and b) TEP coefficient measurement setup for hydrogen charged HSLA steels.

5. PRELIMINARY RESULTS: Cryogenic Seebeck Measurements

HSLA steels have a ferritic (body-centered cubic) microstructure, in which hydrogen has a diffusion coefficient that is orders of magnitude higher than in austenitic (face-centered cubic) microstructure. Because hydrogen has a high mobility, the transfer of steel specimens from the hydrogen charging system to the thermoelectric power measurement system requires a special procedure. The HSLA steel specimens are put into liquid nitrogen was used to immobilize the diffusible hydrogen in these specimens until the TEP coefficient measurements began. Preliminary hydrogen content results on HSLA steels are shown and discussed below.

The hydrogen content of the as-received HSLA steel specimen was 0.52 ppm (Leco Hydrogen Determinator). This as-received HSLA steel specimen was then charged with hydrogen at 1123 K (850 °C) for 48 hours at a pressure of 200 psig. A continuous thermoelectric power measurement of hydrogen content was conducted for a series of specimens in a time interval of 250 minutes. Between the first and second measurements, a large reduction of total hydrogen content (about 13 ppm hydrogen) occurred in the specimen in a period of less than ten minutes (Figure 3), giving direct evidence that the hydrogen distribution in the specimen is not uniform and a large amount of hydrogen is in solution near the surface. The hydrogen trapped on the surface area can easily and quickly diffuse out after the specimens are taken out of the liquid nitrogen. After ten minutes from the start of the

measurement, the rate of hydrogen evolution began to slowly decrease and then became constant at a particular value. The rate of hydrogen evolution began to slow down because more diffusion time is necessary for hydrogen to travel from the middle of the specimen to the surface. It is not reasonable to conclude that the remaining hydrogen is all trapped because the specimens were not baked, and a small amount of diffusible hydrogen could still remain in the specimens after a waiting time of 250 minutes.
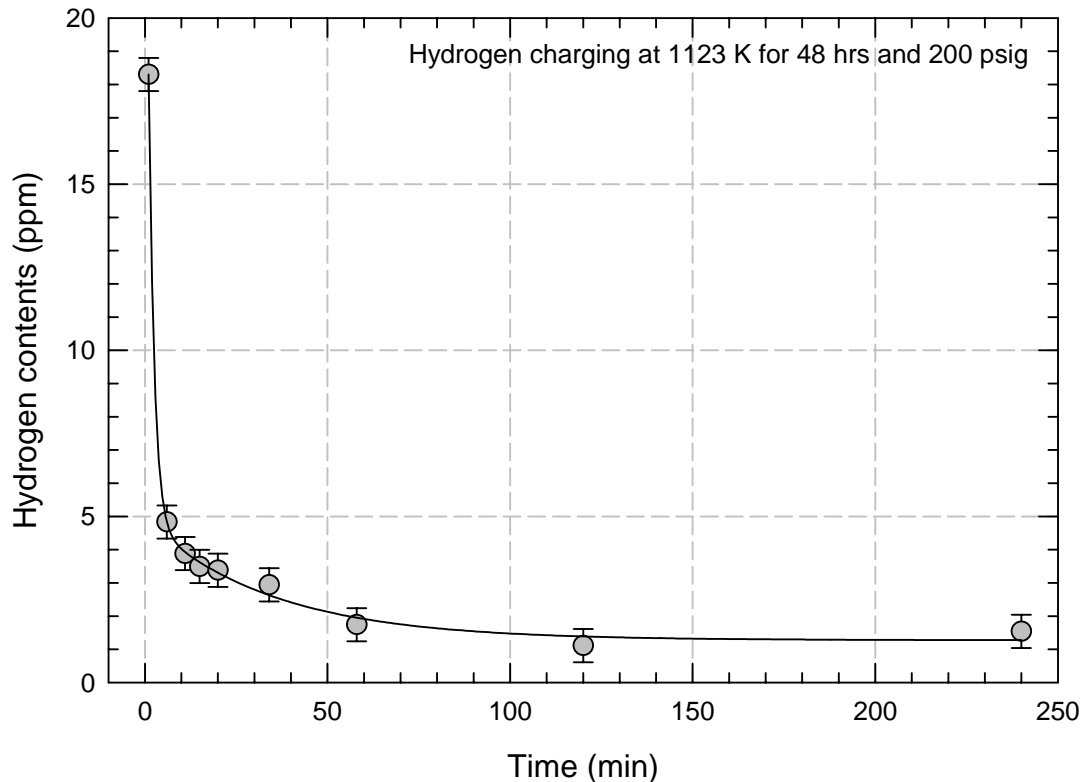

Figure 3. Experimental hydrogen evolution curves measured by the LECO RH-404 hydrogen determinator. All of the specimens were taken out from the liquid nitrogen at the same time and placed in air until the hydrogen content measurements began.

The thermoelectric power coefficient results for the as-received and the liquid nitrogen quenched HSLA steel specimens (without hydrogen charging) are shown in Figure 4(a). The thermoelectric power coefficient quickly decreases from 4.9 to 4.6 (μV/ ^{o}C) in one minute. After one minute, no significant changes in the thermoelectric power coefficient are observed up to a time span of 200 minutes. The large changes in the first minute is mainly due to specimen temperature changes because the specimen was held in liquid nitrogen and then the temperature began to rise to room temperature.
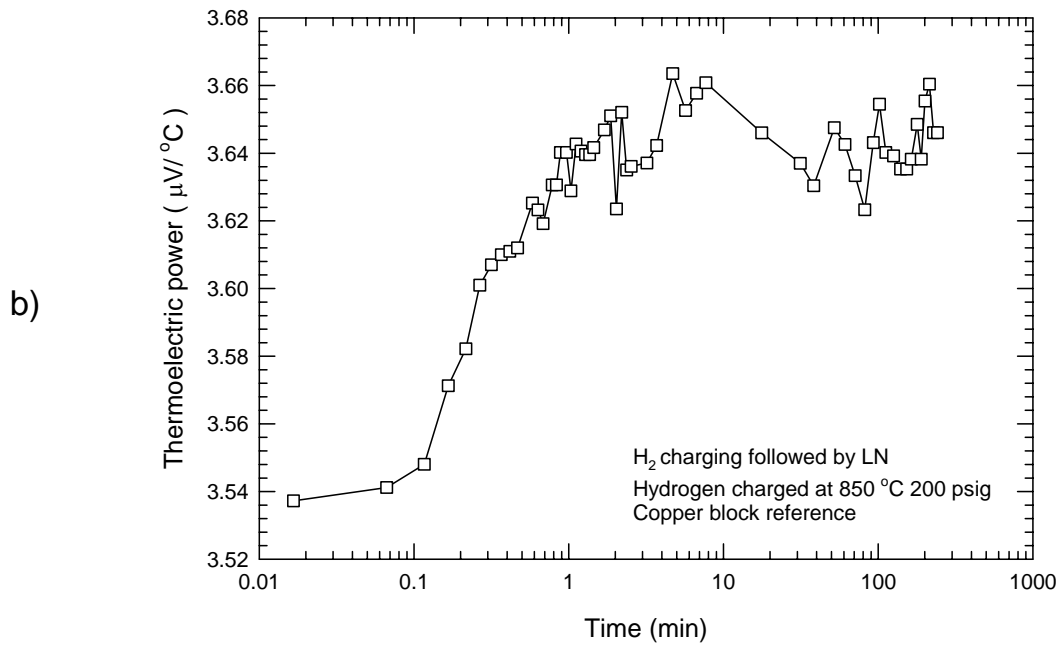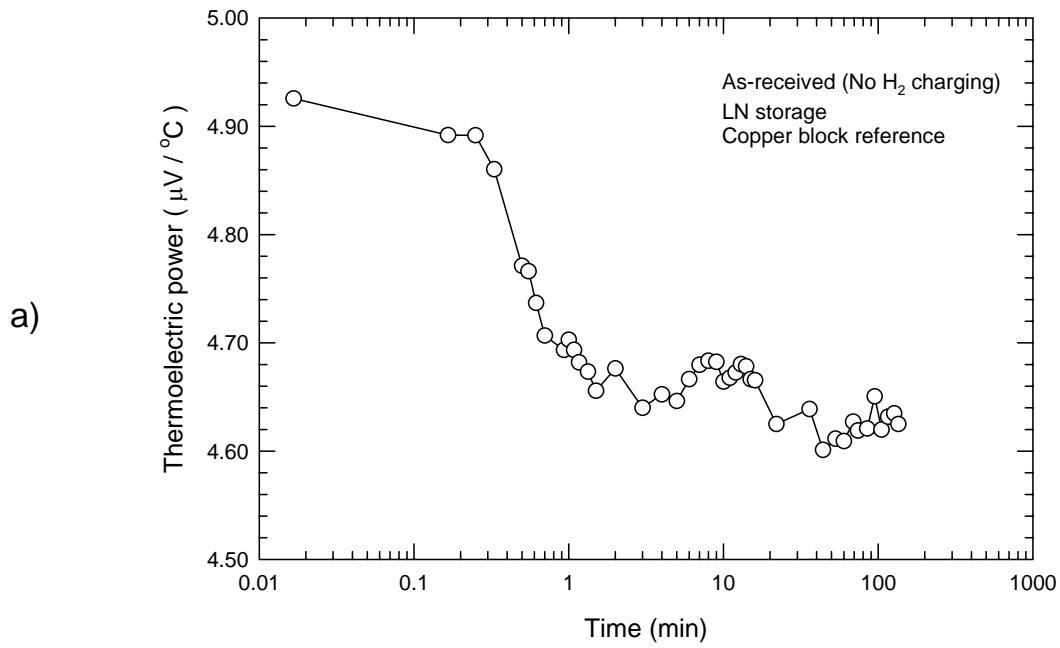
a)

b)

Figure 4. TEP coefficient measurement for HSLA steel (a) as received specimen (b) hydrogen charged specimen. : LN = Liquid Nitrogen

Figure 4(b) shows the thermoelectric power coefficient of the hydrogen-charged HSLA steel specimen. The main difference between the as-received (Figure 4 (a)) and the hydrogen-charged (Figure 4 (b)) thermoelectric power plots are the slope of the curves. The as-received (without hydrogen-charging) curve has a negative slope and decreases with time within two minutes as the specimen warms up from liquid nitrogen to room temperature. The thermoelectric power coefficient of the corresponding hydrogen-charged specimen is positive and increases with time as it warms up from liquid nitrogen to room temperature. There is a huge difference in the thermoelectric power coefficient in the very low temperature range (about $-140^{o}C$) between uncharged and charged specimens. It is very important to notice that there is a large thermoelectric power coefficient difference at low temperature, even though no variation is observed at the room temperature range. This result indicates that the thermoelectric power coefficient can be amplified at low temperatures, resulting in a large deviation in the thermoelectric power coefficient corresponding to the hydrogen-charged HSLA steel.

Figures 4 (a) and (b) show that the thermoelectric power coefficient at room temperature is different between the as-received and the hydrogen charged specimens. This result could be caused by the hydrogen charging process because the specimens were heated to $850^{o}C$ and then were quenched, which results in microstructural changes. In addition, trapped hydrogen in the HSLA steel specimen may also contribute to small changes in the thermoelectric power coefficient.

The thermoelectric power coefficient of the as-received HSLA steel specimen without hydrogen charging is shown in Figure 5 (a). This measurement was made using an iron reference probe to see if there would be an increase in the sensitivity in the thermoelectric power measurement. The thermoelectric power coefficient is constant for a time span of 100 minutes. The result of the thermoelectric power coefficient for the as-received and the liquid nitrogen quenched HSLA steel specimen (no hydrogen charging) is shown in Figure 5(a). The thermoelectric power coefficient result are not much different utilizing a iron reference probe as compared to the copper reference probe in the above measurements. The low temperature curve shows a negative slope and decreases with time within two minutes. The thermoelectric power coefficient of the corresponding hydrogen charged specimen is positive and increases with time (Figure 5(b)). There was no direct evidence of any advantages in using an iron reference material rather than copper reference material. Also, the sensitivity at room temperature does not appear to be improved significantly.

This observation suggests that a practice of cooling a small spot on the pipe and measurement of the thermoelectric power coefficient systematically as the spot warms up will allow an assessment of the hydrogen content in pipe. This will require extensive hydrogen charging and measuring to correlate the thermoelectric power measurement and methodology for future hydrogen assessment on pipe.
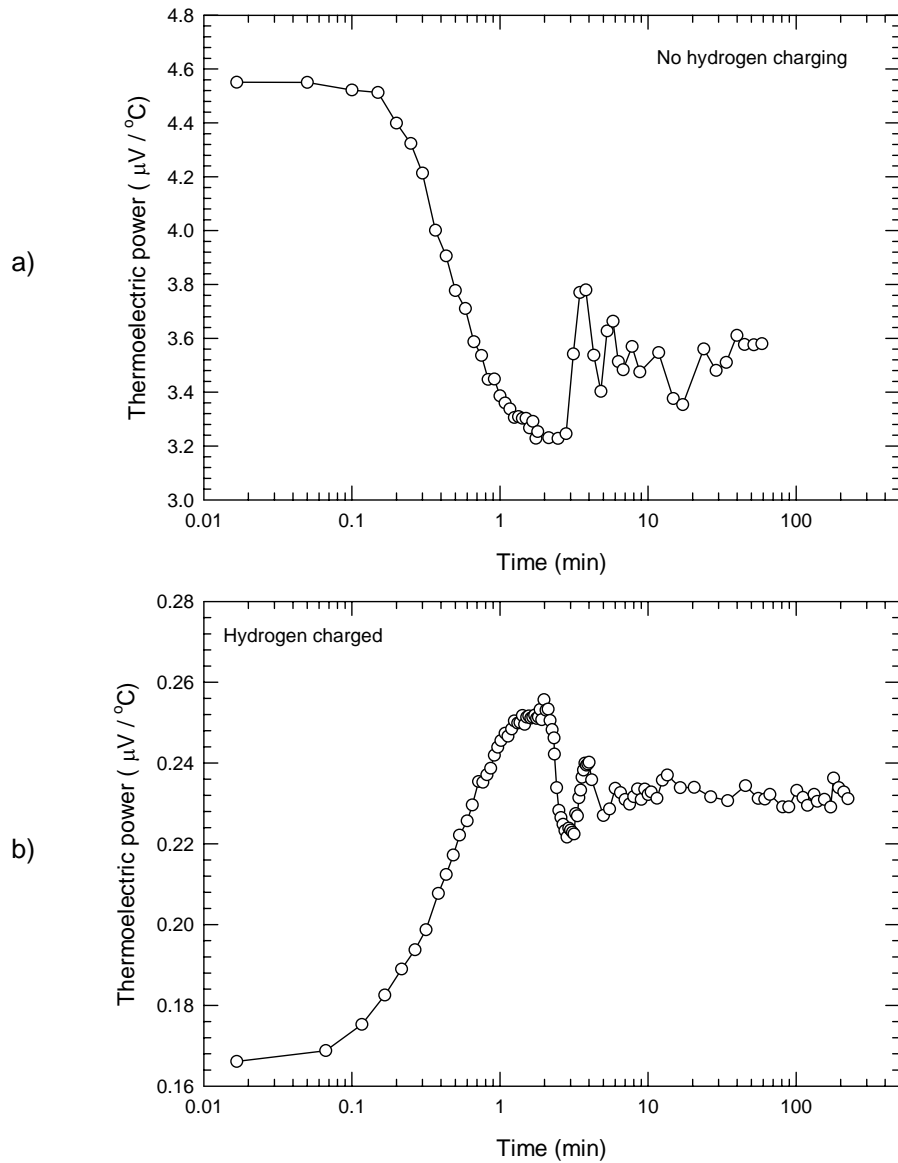
Figure 5. The TEP coefficient measurement for a) as-received and b)
hydrogen charged HSLA steel with iron block reference. Hydrogen was
charged at 1123 K (850 °C) for 48 hours at pressure of 200 psig.

6.   PRELIMINARY RESULTS: Dynamic Seebeck Measurements

To correlate TEP coefficient values with various hydrogen content levels in HSLA steel welds, measurements of actual diffusible hydrogen of welded HSLA steel with increasing hydrogen concentration in shielding gas were conducted according to standard procedures. The hydrogen content of the argon shielding gas was increased to a level of 6 percent by volume. The welding parameters were kept same as described in experimental procedures. Other hydrogen contents, 1, 3, and 5 vol. pct. in shielding gas, were welded, and TEP coefficient measurements were conducted to correlate with diffusible hydrogen content. The probe type TEP measurement system was used and temperature difference between two probes were maintained around 10 $^{\circ}$C. The welded sample was quenched in the liquid nitrogen right after welding, then the measurement was started before temperature reached -100°C.

The results of TEP coefficient measurements of these welded specimens are shown in Figure 6. As diffusible hydrogen content increases, each TEP coefficient curve move to lower level, systematically. These results suggest that the plot of TEP coefficient as a function of either time can be used to curve fit a standard plot to determine the resulting diffusible hydrogen content for steel weld metal.

An attempt can be made to correlate the slope of the TEP coefficient curve to the initial diffusible concentration in the sample. The steady state portion of the curve could be assumed to be proportional to the flux of hydrogen from the weld metal. To investigate this possibility, theoretical curves will be generated using an equation derived from the error function $erf(x)$ as shown in Equation 5. The error function is a mathematical formula associated with a normal Gaussian distribution and occurs often in engineering applications.

$$ erf(x) = \frac{2}{\sqrt{\pi}} \int_0^x e^{-w^2} dw $$

[5]

The diffusion was assumed to occur from a semi-infinite plane sheet with auniform initial concentration C_o through out and a constant surface concentration of zero. For this case, the solution for the error function equation takes the form:

$$ M_t = 2C_o \left(\frac{Dt}{\pi} \right)^{1/2} $$

[6]

where M_t is the amount of hydrogen, D is the diffusion coefficient for hydrogen in a particular medium, C_o is the initial concentration and t is time. Solutions can be generated for different initial concentrations as a function of time.

By using this approach, field practitioners may take the TEP coefficient measurement device and measure the TEP coefficient value of actual welds in low temperature by recording a specimen temperature. The measured TEP coefficient value can be compared with a plot of the TEP coefficient as a function of time, and basically indicates the hydrogen content in the welds. This approach using TEP coefficient measurement at low

temperature makes diffusible hydrogen content measurement much easier and faster. The time required for measurement is about thirty times faster as compared to conventional standard diffusible hydrogen measurement methods.
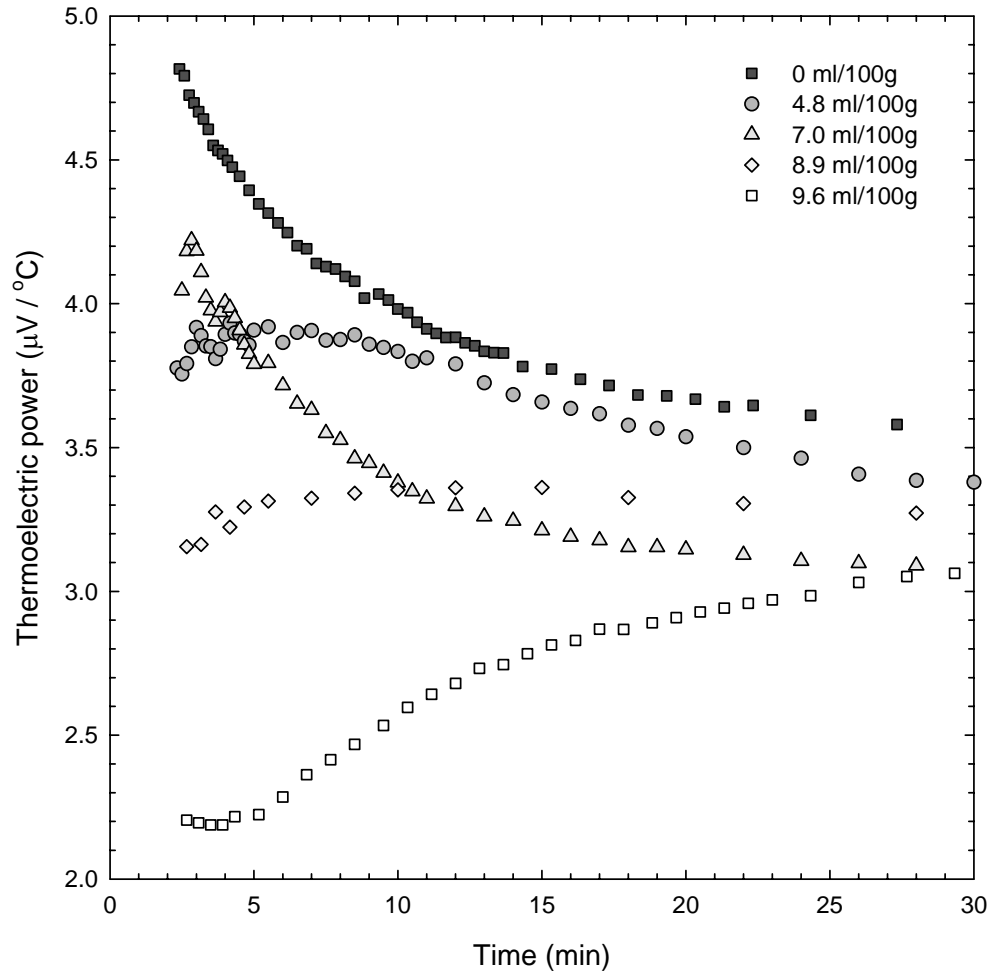

Figure 6. Measured TEP coefficient of welded HSLA steel with five different hydrogen content levels (0, 1, 3, 5, and 6 vol. pct.) in shielding gas for thirty minutes. Actual diffusible hydrogen content is shown in legend. Welding condition: 120 Amps, 1 mm/s travel speed, ice water quenching, and liquid nitrogen storage.

Figure 7 presents the measured TEP coefficient as a function of specimen temperature. Each curve shows linear relationship between the TEP coefficient and the sample temperature when TEP coefficient was plotted as a function of sample temperature. These results indicate that each TEP coefficient curve represents amount of diffusible hydrogen in HSLA steel welds. Therefore, by recording both the TEP coefficient value and specimen temperature for diffusible hydrogen measurement practice, instantaneous amounts of diffusible hydrogen for weld metal can be obtained. The TEP coefficients of fixed sample temperature, such as -60 and -40 ^{o}C, were taken and plotted as a function of diffusible hydrogen content. The results are shown in Figure 8a and b. The results indicate that TEP coefficient is relatively linear with amount of diffusible hydrogen in welded HSLA for both sample temperature of -60 and -40 ^{o}C.
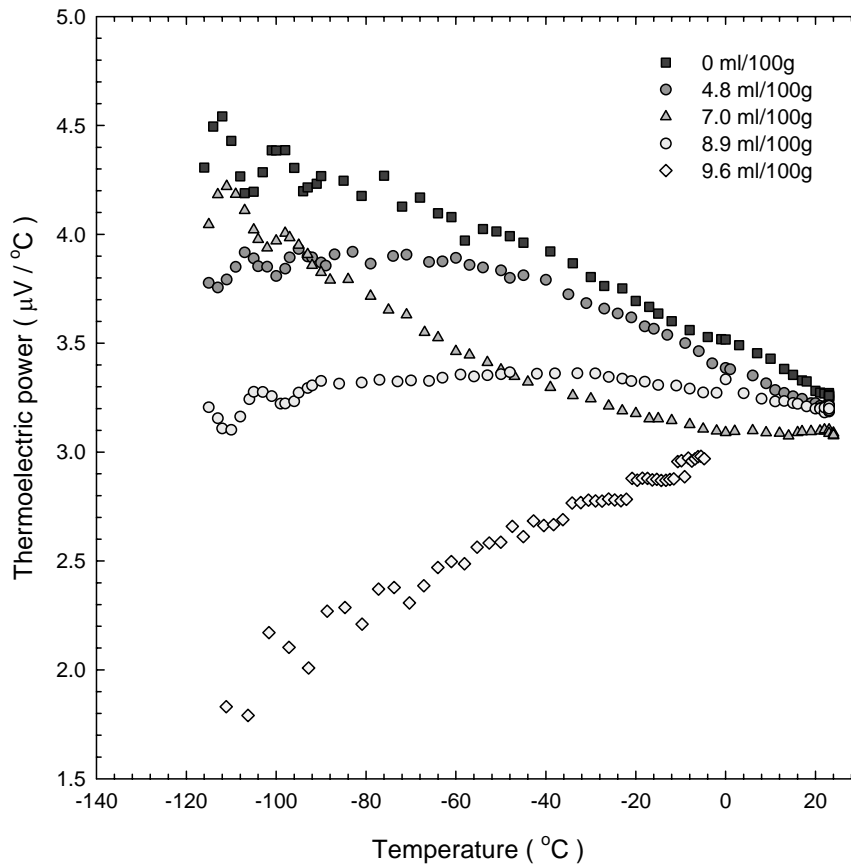

Figure 7. Measured TEP coefficient as function of specimen temperature
for all five welded HSLA steel specimens.

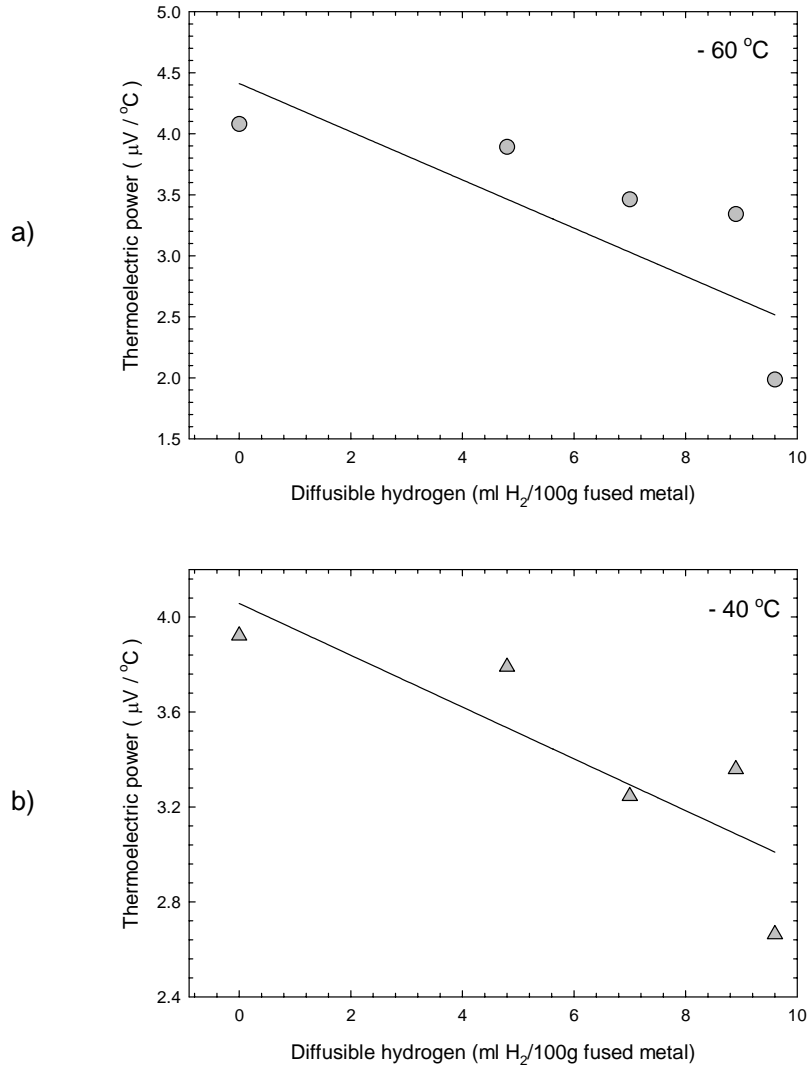Figure 8. Measured TEP coefficient as a function of hydrogen content vol.
pct. in shielding gas at specimen temperature of a) -60 and b) -40 $^{\circ}$C.

Experimental difficulties appear to create poor reproducibility of test results.
Because the liquid nitrogen quenched specimen is placed in a measurement set-up,
the temperature controllers are immediately trying to maintain the differential
temperature (10 $^{\circ}$C), and it takes approximately 5-10 minutes to achieve the stable
differential temperature of 10 $^{\circ}$C. Also, the contact probe pressure on specimens is
found to be a very critical issue at low temperatures.

Other approaches include making TEP coefficient measurements comparing
specimens welded with zero hydrogen in shielding gas and those with 3, 5, and 6
vol. pct. hydrogen in argon shielding gas was taken to correlate with the diffusible
hydrogen content at several temperature. The difference in TEP coefficient between

each curve at fixed temperature can be directly correlated to the amount of diffusible hydrogen or initial hydrogen content of sample. As shown in Figure 9, TEP coefficient was increased with increasing diffusible hydrogen content.
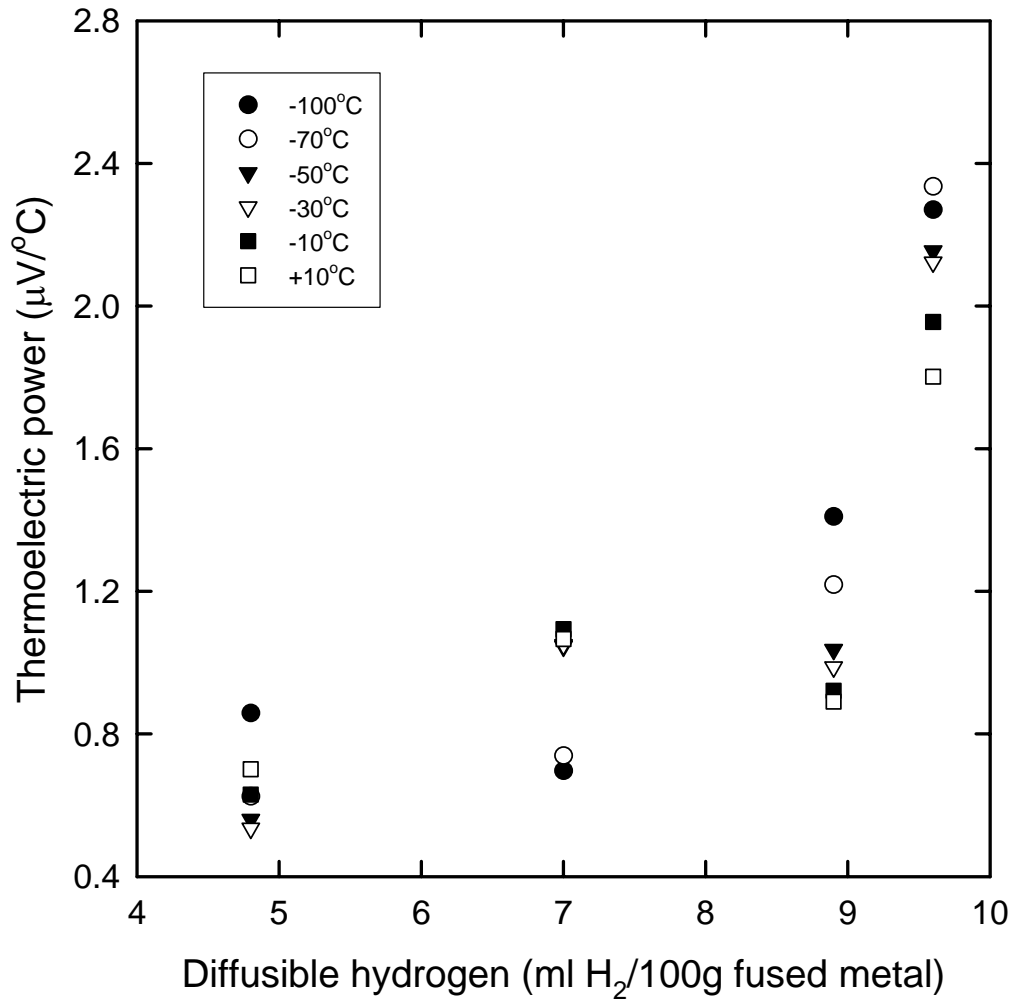

Figure 9. Measured TEP coefficient as a function of diffusible hydrogen content. The TEP coefficient shown in plot was differential values subtracted from TEP coefficient of zero diffusible hydrogen samples.

7. POTENTIAL UTILIZATION

These are preliminary results that suggest that thermoelectric power can potentially be used to assess hydrogen on line pipe, but further work needs to be done to work out a practice and to qualify this practice as a measuring technique to assess hydrogen.

8. REFERENCES

1) Park, Y.D., Lasseigne, A.N., Kaydanov, V.I., Olson, D.L., 10th CF/DRDC Meeting on Naval Applications of Materials Technology, "Thermoelectric Diagnostics for Non-Destructive Evaluation of Materials", CRDC, Dartmouth, NS, Canada, May13-15, 2003, pp. 648-666.

2) Kasap, S., "Thermoelectric Effects in Metals: Thermocouples", e-booklet, electronicmaterials.usask.ca/server/kasap/Samples/Thermoelectric-Seebeck.pdf, (1999).

3) Lavarie, N., Merlin, J. and Sardoy, V., "Study of Ageing in Strained Ultra and Extra Low Carbon Steels by Thermoelectric Power Measurement," (2000), Scripta mater., 44, pp 553-559.